Dear members of the Editorial Board,

First of all, we would like to thank the handling topical editor, the reviewers and all participants in the open discussion for their constructive comments and we would like to state that the format of open discussion proved to be very constructive and helpful. We particularly would like to acknowledge the help of referee Henry (reviewer #3) who not only made helpful comments but also made data available to us. He gave us access to the improved gravity data set TOPEX published by Kende et al. (2017) and to the higher resolved bathymetry of the Marmara Sea. Only thanks to this generous sharing of data we were able to address the main concerns of reviewer #2. We would also like to thank reviewer #2 for revising his/her recommendation towards “major revisions” instead of “reject”.

In our revised version we attempt to address all concerns raised by the reviewers and provide new results considering the full amount of accessible observations. Before we explain how we have addressed the specific concerns of the reviewers in detail, we would like to give a short summary of the additional work that went into the revised version of this manuscript:

We have revised the structural model by implementing the higher resolved bathymetry provided by referee Henry.

We tested the sensitivity of our results by calculating a series of “best-fit models” with respect to both gravity data sets and present a detailed discussion of these results. This quantitatively illustrates how robust the results are and in which range uncertainties are involved.

We have included the additional hypotheses concerning the origin of the modelled high-density bodies in the discussion considering the references suggested by the reviewers.

Please find enclosed our detailed answers to the reviewers’ comments.

In summary we hope the reviewers find their concerns satisfactorily addressed and that the revised manuscript can be accepted for publication.

Yours sincerely
On behalf of all co-authors,
Ershad Gholamrezaie

# Comments to M. Rodriguez, Referee #1, rodriguez@geologie.ens.fr

#Review of the manuscript: 'Crustal density model of the Sea of Marmara: geophysical data integration and 3D Gravity Modelling' By Ershad Gholamrezaie et al. For Solid Earth. This is a beautiful and thorough study about the crustal structure of the Marmara Sea with strong implications for the understanding of the geology of the area and the segmentation of the fault system. The study is clear, well written, with nice figures. The link with seismic and tomography studies makes your 3D crustal model very convincing. I therefore recommend the publication in Solid Earth. However, I have a few minor comments, questions and suggestions.

We thank the reviewer for the encouraging review.

## Scientific comments:

#The definition of the pre-kinematic and syn-kinematic sediments is a bit unclear and somehow difficult to relate to the complex geology of the area. What I do not understand is if this terminology refers to the timing of localization/propagation of the North Anatolian Fault, the opening of the Marmara Sea, or the onset of the Main Marmara Fault. . .or maybe all this stages together? I understand that the prekinematic sediments refers to the deposits older than Late Cretaceous, but there are also some tertiary sediments (Eocene) that were unrelated to the history of the North Anatolian Fault. Do you link these sediments with the pre or syn-kinematic history? You should dedicate a full paragraph where you explain clearly this terminology, and make a clear link with the geological episodes in this area. This terminology is sometimes confusing.

We thank the reviewer for pointing this out. We have clarified the formulation to make clear what we mean with syn-kinematic/pre-kinematic sediments (see page 6 lines 8-29 and page 7 lines 15-22 to in revised MS).

With syn-/pre-kinematic we mean with respect to the opening of the Marmara Sea. How far this is related to activity of the NAFZ needs to be discussed. The thickness variation of the youngest sediment unit indicates a clear spatial relationship with respect to two points: (1) with the present-day sub-basins of the Marmara Sea as imaged by bathymetry and (2) with respect to the trace of the MMF in that the latter partly coincides with the margin of the sub-basins. On the other hand, the thickness of the pre-kinematic sedimentary unit displays pronounced minima in the domain of the present-day Marmara Sea, which indicates that this unit has been disrupted during the formation of the Marmara Sea.

#I have found the link with seismic profiles and tomography very convincing (especially the link with Becel et al. and Laigle et al.): Maybe you should add a figure summarizing what we have learned from these studies (i.e. a few cross sections). Some readers may not be familiar with these studies and find all the related sections difficult to follow.

We agree with the reviewer and have added an example for a seismically derived structural cross-section (new Fig. 4), that we also compare to cross-sections in the same position through the three presented end-member models (new Fig. 10).

#One of the strongest result is the identification and mapping of the high density body, with a density ~3. However I feel that the discussion about its origin is incomplete. You link these bodies to deep magmatic activity coeval with the activity of the North Anatolian Fault but the mechanism at the origin of these high density bodies is unclear. Shear heating of the lower crust or the top of the lithospheric mantle? How can you be sure that the formation of these high density bodies is related to the activity of the North Anatolian Fault? What are the arguments? An alternative may be to consider these high density bodies reflects the intra-pontides suture zone. Parts of this suture zone has been mapped onland (see a synthesis in LePichon et al 2014), but the offshore mapping remains unclear. I wonder if what you identify may actually be some ophiolites or metamorphic rocks trapped along this suture zone. In terms of density, ophiolites are >3, some metamorphic rocks can reach the same density. For some insights about the intra-pontides suture zone, I suggest the following papers: Okay and Tüysüz, 1999; Robertson and Ustaömer, 2004. If the ophiolites/suture zone hypothesis is correct, then it means that structural inheritance strongly controls the SED segmentation of the North Anatolian Fault in this area. It would also strongly emphasize some previous

suggestions of Celal Sengör, who proposed that the localization of the North Anatolian Fault is strongly influenced by the intra-Pontides suture zone.

Indeed, the discussion was rather brief in the first version of the MS and we agree that there are more concepts to include in the discussion on the origin and nature of these bodies. We thank the reviewer for pointing us to the respective literature, that we have studied. We now provide a more extended discussion on this point, also considering hypotheses put forward in previous work (see page 13, Sec 5. Interpretation and discussion of the best-fit models). We, however, prefer to stay careful in this discussion, as our results are not suited to discriminate between several possible interpretations. We therefore discuss the implications of the different possible interpretations concerning the origin of the high-density bodies but refrain from favouring one. Regarding the intra-pontides suture zone and its relation to the high-density bodies we added the following paragraphs:

Page 15 line 16: "As we do not have further evidence for a magmatic origin of the high density bodies, other possible interpretations of these domains may be considered. For example, these high density bodies could represent inherited structures of former deformation phases such as ophiolites along the intra-Pontide suture that has been mapped on land, but have not yet been explored offshore (Okay and Tüysüz, 1999; Robertson and Ustaömer, 2004; Le Pichon et al., 2014; Akbauram et al., 2016). The two different emplacement mechanisms would have opposing consequences for the propagation of the North Anatolian Fault. The magmatic origin would be consistent with crustal weakening in these domains, whereas the ophiolite origin would imply the opposite. In both cases, however, a local strength anomaly in these domains would be the consequence that could be related to the bending of the fault. Whatever the origin of these bodies, their mafic composition would imply that they represent domains of higher strength in the present-day setting."

Page 15 line 26: "In Model-III as the alternative best-fit model for the Improved–TOPEX gravity dataset, the sixth unit has been calculated identical to the geometry of Model-I (Fig. 9a) but with the average density of 2890 $kg.m^{-3}$ as similar to average density of the lower crust. This density value is consistent with the average density value of intermediate to mafic metamorphic rocks such as granulite (Christensen and Mooney, 1995). In this case, these two dome-shaped bodies may be interpreted as trapped metamorphic rocks along the Intra-Pontide suture zone that spatially correlates with the MMF propagation (Şengör et al., 2005; 30 Le Pichon et al., 2014; Akbauram et al., 2016)."

## Detailed comments:

#the title reads a bit long: I suggest something like '3D crustal density model of the Marmara Sea'

We agree and have changed the title accordingly.

#Geological setting: lateral escape of Anatolia is not only the result of Arabia indentation, there is also a link with the retreat of the Hellenic trench, see Faccenna et al 2006 EPSL for an elegant synthesis

Thanks for pointing this out, we have complemented in the text accordingly:

page 2 line 25: "In the large-scale plate-tectonic framework of Asia Minor, the NAFZ accommodates the westward escape of the Anatolian plate in response to the northward motion and indentation of the Arabian plate into Eurasia and westward enlarging of the deep slab detachment beneath the Bitlis–Hellenic subduction zone (Fig. 1a: McKenzie, 1972; Şengör et al., 2005; Faccenna et al., 2006; Jolivet et al., 2013)…"

#Geological setting: page3 Line 25. LePichon et al 2003 provide some observations suggesting the present-day context is pure strike slip, not transtensional (no oblique extensive stresses), except in the area of Cinarcik where the bend of the fault favors extension:

Scanning the debate on this issue we found that there is contradictory interpretation of the few true stress observations. Hergert and Heidbach (2011) provide plausible arguments for lateral variations in stress regime. We therefore would like to report the full spectrum of the discussion and decided to keep this statement, though complemented by the respective reference. As suggested by the reviewer, the following paragraph was added the revised manuscript:

Page 3 line 24: “In contrast, based on GPS velocity data and surface geological observations, there are also arguments that the kinematics of the MMF correspond to a pure right-lateral strike-slip with the exception of the Çınarcık Basin area that the bend of the Princes Islands segment causes a transtensional setting (e.g. Le Pichon et al., 2003; 2015).’’

#In the discussion, please compare better the improvements of your study with previous ones (Kende. . .etc...)

This has extensively been done, see also answers to reviewers2 and 3.

## Comments related to the figures:

#In the captions, please refer to the meaning of the abbreviations, it is sometimes boring to jump from one figure to another to find the significance.

Done.

#In figure 8: you should number the layers to ease the link with the text (for instance, when you refer to the third layer, the reader has to guess which one is it on the figure...)

Done as new Fig. 10.

#As mentioned earlier, maybe adding some cross sections from previous works (Laigle et al 2008 especially) may help the understanding of your study for a broader audience

Done, new Fig 4.

#I hope you will find these comments helpful and constructive Best regards, Dr. Mathieu

Rodriguez Ecole normale supérieure de Paris

Indeed, we found these comments helpful, thanks again.

#Suggested References:

Faccenna, C., Bellier, O., Martinod, J., Piromallo, C., Regard, V., 2006. Slab detachment beneath eastern Anatolia: a possible cause for the formation of the North Anatolian Fault. Earth and Planetary Science Letters 242, 85-97.

Okay, A.I., Tüysüz, O., 1999. Tethyan sutures of northern Turkey. Geological Society of London, Special publications, 156, 475-515. Robertson, A.H.F., Ustaömer, T., 2004. Tectonic evolution of the intra Pontide suture zone in the Armutlu Peninsula, NW Turkey. Tectonophysics 381, 175-209.

Integrated.

# Comments to RC2: 'Major concerns regarding the gravimetric and bathymetric datasets used in the study cast doubt on the results', Anonymous Referee #2.

We thank reviewer #2 for helpful comments and have earlier directly responded in the open discussion. For completeness we list the main points to the reviewer's comments again here.

The paper addresses the question of the deep crustal structure of the submerged section of the North-Anatolian Fault within the Sea of Marmara, which may have important implications to better assess the earthquake hazard in the highly populated (> 15 Millions inhabitants) Istanbul area. A new crustal-scale 3D density model integrating geological and seismological data is presented, based on additional 3D-gravity modelling. The major result is that the crust appear to be crosscut by two large, dome-shaped mafic high-density bodies (average density of 3050 kg.m-3) of considerable thickness above a rather uniform lithospheric mantle (3300 kg.m-3 ). It is to be noted here that the location of these two bodies coincides with the location of two major escarpments: below the Tekirdag and the Cinarçik escarpments, respectively (Figure 9c). As a conclusion, the authors then suggest that these high-density bodies control the rheological behaviour along the NAFZ, and consequently, influences fault segmentation and propagation dynamics. The paper is well presented and well written. However, there are major concerns regarding the dataset, both for gravimetry and for bathymetry from the offshore domain in Sea of Marmara.

1) For gravity, the authors use the EIGEN-6C4 dataset (Förste et al., 2014), which is a combined global gravity field model up to degree and order 2190 correlating satellite observations (LAGEOS, GRACE, GOCE) and surface data (DTU 2'x2' global gravity anomaly grid). At the scale and wavelengths concerned by the present study: 1) the DTU 2'x2' global gravity anomaly grid, based on satellite altimetry, is predominant and 2) the density contrast is at the sea-bottom interface is of critical importance. It is highly regrettable that no discussion is presented to compare the free-air gravity anomaly from ship-board gravimeters and the satellite derived gravity data used in the present paper for the offshore domain. In Figure 2 of Kende et al (note missing reference: J. Geophys. Res. Solid Earth, 122, 1381–1401, doi:10.1002/ 2015JB012735), the differences between the two datasets are shown along a 130 km long profile, oriented along the strike of the main fault, following the deeper parts of the Sea of Marmara. This profile represents the most favourable configuration for using gravity from radar altimetry. Still, there are major differences. The N-S profiles (B-B' and C-C') shown in Figures 7 and 8 of the present submission represent the worst configuration for satellite altimetry-derived gravity, as they cross sharp escarpments bordering the Tekirdag and Cinarçik basins, which are expected to produce important effects on the gravity signature. A comparison between satellite gravity and ship-board gravity must be presented and the effects related to the use of altimetry-derived gravimetry must be discussed.

(1) The first major concern of reviewer #2 is that we have used the wrong gravity data set. In particular, the reviewer mentions the higher resolved data set introduced in the Kende et al. 2017 paper. We would like to repeat that it was not the scope of this paper to quality check published and downloadable gravity data, as these went through a review process before publication. We wanted to explore, what additional understanding can be gained if such data is integrated with previous models, other geophysical data and forward 3D gravity modelling. We agree that there is a mistake concerning the correct referencing of the Kende et al., 2017 paper and apologize for this. The reference was corrected and substantial discussion has been added to MS with respect to both the gravity data set as well as the bathymetry presented by Kende et al. (2017).

For the revised version of this paper we have tested the sensitivity of our results with respect to both data sets: Förste et al. (2014) and Kende et al. (2017). We had used the publicly available data set EIGEN-6C4 (Förste et al., 2014) in the initial submission because it covers the onshore and offshore parts of the study area. The higher resolved dataset the reviewer recommended to use instead and presented in Kende et al. (2017) was not publicly available for the initial submission. Fortunately, thanks to support from reviewer #3 P. Henry, the Kende at al. (20179 datasets was made available to us and we could extend our analysis beyond our initial reply to reviewer #2 in the open discussion. We explored the gravity response of different model configurations with respect to both data sets and present 3 "best

fit" endmember models in the revised manuscript that illustrate the sensitivity of the results. In addition, we supply further details in the Supplementary Information.

Nevertheless, we thank the reviewer for pointing out this discrepancy between the different gravity data sets and we carefully have checked which differences we obtain between our model adjusted for the EIGEN-6C4, a model adjusted to the dataset of Sandwell et al. (2014) or a model adjusted for the data set of Kende etal. (2017). We can confirm that the high-density bodies are still required, though fitting the different gravity datasets would require the high-density bodies to be slightly smaller in size or density (non-uniqueness of gravity). We have included a detailed comparison in the paper in the revised version and thus document the related uncertainties. Nevertheless, there are consistent findings in our study and the study of Kende et al. (2017). In particular, the latter also show the need for deep compensation of the sedimentary fill, however, the authors propose to achieve this implementing as uplift of the Moho in the domains of our lower crustal high density bodies. In detail, they propose local shallowing of the Moho – and therewith also high-density bodies that are 5 km thick with a density of 3330kg.m$^{-3}$, compared to +15 km of density 3000 kg.m$^{-3}$ in our initial model, assuming a laterally uniform density of the crystalline crust. This is supporting our results rather than discarding them. We have added a quantitative comparison in the new manuscript in this respect (page 12: Sec 4.2.3. Best-fit models, and page 16: Sec 5.3. Comparison with published 3D density model).

Seismological data used for model construction (e.g. Becel et al., 2009) indicate that no such pronounced Moho uplift is present in the domains of our high-density bodies, a point also admitted by Kende et al. (2017). They critically review this misfit with their model and mention uncertainties in the seismic data as possible reasons for the misfit. However, if these uncertainties in the seismological constraints are small, the derived Moho uplift may not be there and the crystalline crust may not be as uniform as suggested by Kende et al.'s gravity modelling results. Moreover, the limited available seismological observations (Becel et al., 2009; Karabulut et al., 2013; Bayrakci et al., 2013) indicate that seismic velocities vary within the crystalline crust. In particular, an increase in seismic velocities is found in the regions where the uppermost part of the high-density bodies modelled in our study are located (New Fig.4 and Fig. 10)

Finally, the locations of the lower crustal high-density bodies also correlate spatially with a positive magnetic anomaly (Ates et al., 1999;2003; 2008), also suggested to consult by reviewer #3. This indicates that some mafic lithology is present below the non-magnetic sediments. Thus, assuming a uniform density and a +/- constant thickness of the upper and lower crystalline crust separated by an interface running parallel to the Moho is difficult to justify.

In summary all evaluated gravity data sets require the presence of local bodies of higher than average crustal density in the deeper crust. If these are large and characterized by a smaller density contrast to the surrounding crystalline crust or smaller and of higher density remains unclear. Here, additional deep seismic data would help to reduce non-uniqueness.

2) For topography-bathymetry (shown figure 1c), the authors use a dataset exported from 1 Arc-Minute Global Relief Model (Amante and Eakins, 2009), which integrates the 30 arc-second grid obtained from NASA's Shuttle Radar Topography Mission (SRTM) and a bathymetry dataset from the MediMap Group, 2008. Bathymetric grids from the Medimap group have a 1 km grid-node spacing. Compared to high-resolution grids based on shipboard, multibeam echsounders (e.g. [Le Pichon et al., 2001]), such grids are expected to smooth considerably the bathymetry, when sharp escarpments are present, particularly at the Western Tekirdag and the Northern Cinarcik escarpments. A smoothen bathymetry at escarpments may induce unwanted effects in gravity modelling, by introducing artificially the need of compensating high density bodies at depth. The concerns listed above on both the gravimetry and the bathymetry datasets, cast serious doubts on the reality of the two high density bodies found by the authors. Besides these two major issues, a geological discussion on the implications of the results is cruelly missing (gravity model solutions are not unique; geological criteria represent the best guides for discussing non-unique solutions). In conclusion, for the above reasons, I do not recommend publication of the submitted paper in Solid Earth Discussions. A substantial effort is needed: 1) for testing the relevance of the gravity model they use in the case of the Sea of Marmara (particularly due to the presence of sharp escarpments) 2) for testing the relevance of

the bathymetric grid 3) for presenting an in-depth, geological discussion for discriminating the different (non-unique) results.

(2) This other main point of the reviewer is that we do not consider the right bathymetry, in particular the one presented in Kende et al. (20179 or in more detail in Le Pichon et al. (2001). Though we are sure that this would not be of primary importance, given the horizontal resolution of our lithosphere-scale model we have implemented this bathymetry into the revised models. Again we would like to acknowledge the generous supply of this data set by reviewer #3, P. Henry. The differences with respect to the initial model related to this modification were indeed in the range of a few mGals and thus do not question the presence or absence of deep bodies causing a response of at least several tens of mGals and tens of km in wavelength. Accordingly, considering the higher resolved bathymetry and the higher resolved gravity data has helped in defining sharper boundaries of the high density bodies but their presence was still required.

The reviewer also asks for more discussion of the geological implications of our results, which was also suggested by the other reviewers. We have therefore added discussion on the consequences of the different interpretations for the deep structure of the Marmara Sea against the background of previously proposed concepts (page 13-16). This indeed has sharpened the respective parts of the MS with respect to hypotheses for the deformation mechanism that created the Marmara Sea and for the present day distribution of strength in the crust.

# Comments to P. Henry, Referee #3

#This manuscript presents an interesting new hypothesis explaining gravity anomalies in the Sea of Marmara area: the presence of high density bodies within the crust along the North Anatolian fault zone. However, the manuscript does not yet provide a fully convincing demonstration that the presence of these bodies is required by the available data. Owing to the non-uniqueness of gravity inversion solutions, and to the limitations of the currently available constraints from seismology, the gravity modeling alone cannot prove the existence of the high density bodies. Data may also be fit (at least at wavelengths of more than about 30 km) considering relatively small variations of Moho depth that remain compatible with constraints from seismology. The presence of high density bodies, is, however, a sound hypothesis, which can be further supported by considering the geological and geophysical contexts.

We have carried out, as already stated above, more detailed sensitivity studies and have revised the models and interpretations (see answers to editors and reviewers #1 and #2)

#Geological knowledge on the Sea of Marmara area is already integrated in the discussion, but two important points are missing: (1) Ates et al. (1999, 2003, 2008) found magnetic anomalies in the Sea of Marmara area, which they related to the presence of magnetic bodies along the North Anatolian Fault zone. The largest one coincides with the eastern dense body infered in this study. (2) The North Anatolian fault zone follows more or less an ophiolitic suture, and this could explain at least in part the presence of dense and/or magnetic bodies along its track. Heterogeneities in the crust may thus not be a consequence of magmatic intrusions during a rifting event, but be a consequence of the convergent, and then transcurrent, tectonics during the Paleogene. This is already appearent in some of the cited references (e.g. Sengor et al., 2005) and more recent references also exist (e.g. Akbauram et al., 2016).

Thanks for pointing us to the additional publications. We have consulted those and in particular the work on magnetic anomalies was indeed important. We have complemented the discussion with respect to these findings (see page 14-15). In particular, the we added the following paragraph to the manuscript:

Page 15 line 3: “The mechanisms and timing of the emplacement of the high-density bodies are, however, difficult to determine. The modelled density indicates that the high-density bodies represent magmatic additions to the Marmara crust, potentially originating from larger depths that rose buoyantly into domains of local extension. Magnetic anomalies across the Sea of Marmara indicate positive anomalies along the MMF that may be interpreted as magnetic bodies along the fault (Ates et al., 1999; 2003; 2008). In particular, the locations of the high-density bodies beneath the Çınarcık Basin correlate spatially with the maximum positive magnetic anomaly (Ates et al. 2008) which indicates that some mafic lithology is present there below the non-magnetic sediments.”

#My conclusion would be that the gravity anomaly in the Eastern Sea of Marmara is at least in part caused by a mafic/ultramafic sliver in the crust, but it is still unclear to me whether a large high density body is present beneath Tekirdag Basin. I fully agree with the authors that these bodies could be a possible factor controling strain localization within the North Anatolian shear zone and that they predate the Pio-Quaternary transtensional tectonics, but I am not convinced they were emplaced as magnatic intrusions within the continental crust.

Concerning this comment, we agree that the high-density bodies could also represent inherited structures. However, the spatial correlation between the position of these bodies and the thickness maxima in the syn-kinematic sediment distribution is also evident. We have therefore decided to keep the two alternative interpretation scenarios.

#Regarding the discussion with Reviewer #2, I would like to confirm that the Sandwell/TOPEX gravity model has good consistency with the marine data that were collected during Marsitecruise (both used in Kende et al., 2015), and that the Eigen- 6C4 anomaly map used here seems less consistent with these marine data. I would like to encourage the authors to go on with their suggestion to compare models fitting Topex and Eigen-6C4 gravity anomalies. I would be happy to provide the gravity data used in Kende et al. to the authors (hence, do not request to stay anonymous). Ideally, a magnetic model could be added.

This provision of the data was essential for improving our manuscript and this way of receiving feedback is what authors ideally would wish for. As detailed in the comments to the other reviewers we have carefully carried out the comparison suggested by the reviewer and our work has greatly profited.

We agree that a magnetic model would be ideally complementing this work, but as no robust information on magnetic susceptibilities was available to us, we decided to postpone this to future work.

#References:

Akbayram, K., S¸ engör, A. M. C., & Özcan, E. (2016). The evolution of the Intra-Pontide sutureâˇA´r: Implications of the discovery of late Cretaceous – early Tertiary mélanges. In R. Sorkhabi (Ed.), Tectonic Evolution, Collision, and Seismicity of Southwest Asia: In Honor of Manuel Berberian's Forty-Five Years of Research Contributions: Geological Society of America Special Paper 525 (Vol. 525). https://doi.org/10.1130/2016.2525(18)

Ates, A., Kayiran, T., & Sincer, I. (2003). Structural interpretation of the Marmara region, NW Turkey, from aeromagnetic, seismic and gravity data. Tectonophysics, 367, 41–99. https://doi.org/10.1016/S0040-1951(03)00044-1

Ates, A., Kearey, P., & Tufan, S. (1999). New gravity and magnetic anomaly maps of Turkey. Geophysical Journal International, 136(2), 499–502. https://doi.org/10.1046/j.1365-246X.1999.00732.x

Ates, A., Bilim, F., Buyuksarac, A., & Bektas, Ö. (2008). A tectonic interpretation of the Marmara Sea, NW Turkey from geophysical data. Earth, Planets and Space, 60(3), 169–177. https://doi.org/10.1186/BF03352780

All references were considered and integrated in our discussion.

# 3D Crustal Density Model of the ~~Sea of~~ Marmara~~: Geophysical Data Integration and 3D Gravity Modelling~~ Sea

Ershad Gholamrezaie[1,2], Magdalena Scheck-Wenderoth[1,3], Judith Sippel[1], Oliver Heidbach[1], and Manfred R. Strecker[2]

[1]Helmholtz Centre Potsdam–GFZ German Research Centre for Geosciences, Potsdam, Germany
[2]Institute of Earth and Environmental Science, University of Potsdam, Germany
[3]Faculty of Georesources and Material Engineering, RWTH Aachen, Aachen, Germany

*Correspondence to*: Ershad Gholamrezaie (ershad@gfz-potsdam.de)

**Abstract.** The Sea of Marmara, in Northwest Turkey, is a transition zone where the dextral North Anatolian Fault Zone (NAFZ) propagates westward from the Anatolian plate to the Aegean plate. The area is of interest in the context of seismic hazard in the vicinity of Istanbul, a metropolitan area with about 15 million inhabitants. Geophysical observations indicate that the crust is heterogeneous beneath the Marmara Basin, but a detailed characterization of the crustal heterogeneities is still missing. To assess if and how crustal heterogeneities are related to the NAFZ segmentation below the Marmara Sea, we develop a new crustal-scale 3D density model which integrates geological and seismological data and is additionally constrained by 3D gravity modelling~~.~~ considering two different gravity datasets including global satellite data and local marine gravity observation. This model indicates that the observed gravitational anomalies originate from significant density heterogeneities within the crust. Two layers of sediments, one syn-kinematic and one pre-kinematic with respect to the Marmara Sea formation are underlain by a heterogeneous crystalline crust. A felsic upper crystalline crust (average density of 2720 kg.m$^{-3}$) and an intermediate to mafic lower crystalline crust (average density of 2890 kg.m$^{-3}$) appear to be crosscut by two large, dome-shaped mafic high-density bodies (~~average~~ density of ~~3050~~2890 to 3150 kg.m$^{-3}$) of considerable thickness above a rather uniform lithospheric mantle (3300 kg.m$^{-3}$). The spatial correlation between the bent segments of the fault and the location of the high-density bodies suggests that the distribution of lithological heterogeneities within the crust controls the rheological behaviour along the NAFZ, and consequently, influences fault segmentation and propagation dynamics.

## 1. Introduction

The Sea of Marmara in NW Turkey is an extensional basin associated with a right-stepping jog in the orientation of the North Anatolian Fault Zone (NAFZ; Fig. 1), a westward-propagating right-lateral strike-slip fault that constitutes the plate boundary between the Anatolian and the Eurasian plates (Fig. 1a; McKenzie, 1972; Şengör et al., 2005). As one of the most active plate-bounding strike-slip faults in the world, and being located in the Istanbul metropolitan area with a population of approximately 15 million, the NAFZ has been the focus of numerous geoscientific investigations over the past decades (e.g. Barka, 1996; Ambraseys, 1970; Stein et al., 1997; Armijo et al., 1999; Şengör et al., 2005; Le Pichon et al., 2015). Several recent

research programs (e.g. SEISMARMARA: Hirn and Singh, 2001: http://dx.doi.org/10.17600/1080050; GONAF: Bohnhoff et al., 2017a: https://www.gonaf-network.org; MARsite: http://www.marsite.eu) have been embarked on to improve the observational basis for hazard and risk assessments in the area of the Marmara Sea.

The Marmara section of the NAFZ, considered to be a 150-km-long seismic gap between the ruptures of two big events in 1912 (M 7.3) and 1999a (M 7.4), is a zone of strong earthquakes (M ~ 7.4) with a recurrence time of approximately 250 years (Fig. 1b and 1c); this section experienced the last ground-rupturing events in 1509 and 1766, suggesting that the fault is mature and a ground-rupturing event might be expected (Ambraseys, 2002; Barka et al., 2002; Parsons, 2004; Janssen et al. 2009; Murru et al., 2016; Bohnhoff et al., 2016a; 2016b; 2017b). There, the potential for a large seismic event is regarded as being high (Bohnhoff et al., 2013; 2017b). A key question is if this 150-km-long seismic gap will rupture in the future in one event or in several separate events due to the segmentation, an issue that will depend a lot on the stress evolution along strike among other forcing factors. In this regard, three-dimensional (3D) geological models are the fundament of geomechanical models, and the distribution of density is of key importance as density controls body forces. Density modelling is generally done by integrating geological information, seismic observations, and gravity data. ~~In the Marmara region, however, 3D gravity modelling has not been at the focus compared with the use of other geophysical methods.~~ Furthermore, gravity models can also help ~~clarify~~to assess the density distribution at greater depth where borehole observations and/or seismic surveys have limitations.

Our study aims ~~at assessing~~to evaluate the deep crustal configuration of the Marmara Sea and surrounding areas. To address the question if there is a spatial relationship between fault activity and the distribution of certain physical properties in the crust, we ~~developed a~~develop 3D density ~~model~~models that ~~integrates~~integrate available seismological observations and ~~is~~are consistent with observed gravity measurements. In a previous gravity modelling effort (Kende et al., ~~2015), after wavelength-depth-related crustal correction,~~2017), an inversion method was applied to calculated the Moho depth below the Marmara region. ~~This study (Kende et al., 2015) revealed that assuming laterally homogeneous crustal layers is insufficient to integrate density heterogeneities.~~ Building on an earlier 3D structural model ~~(sediments; crust; Moho; Fig. 2 and 3)~~ developed to evaluate the stress-strain state in this region (Hergert and Heidbach, 2010; 2011; Hergert et al., 2011), we ~~used~~use crustal and regional-scale forward 3D gravity modelling and seismic data as additional constraints. ~~Here we show~~In addition, we compare and discuss our results with the previously published results of Kende et al. (2017). This comparison confirms that significant density heterogeneities are laterally present within the crust below the Sea of Marmara.

~~Our results from forward 3D gravity modelling point to the existence of~~In particular, we find indications for lateral density heterogeneities within the crust in the form of two local high-density bodies~~. This supports the notion of rheologically strong crustal domains~~ that may influence the kinematics of the NAFZ below the Sea of Marmara.~~ In addition, considering the results of the earlier geomechanical numerical models (Hergert and Heidbach, 2010; 2011; Hergert et al., 2011), we suggest that implementing the high-density bodies in the structural model may change earlier results.~~

### 1.1. Geological setting

In the large-scale plate-tectonic framework of Asia Minor, the NAFZ accommodates the westward escape of the Anatolian plate in response to the northward motion and indentation of the Arabian plate into Eurasia ~~(Fig. 1a~~and westward enlarging of the deep slab detachment beneath the Bitlis–Hellenic subduction zone (Fig. 1a: McKenzie, 1972; Şengör et al., 2005; Faccenna et al., 2006; Jolivet et al., 2013); this has resulted in numerous deformation features along the well-defined trace of the fault and regionally, along the northern flanks of the Anatolian Plateau (Barka and Hancock, 1984; Barka, and Reilinger, 1997; Pucci et al., 2006; Yildirim et al. 2011; 2013).

In the westernmost sector, the NAFZ bifurcates into several strands of locally variable strikes, which has resulted in a mosaic of pull-apart basins flanked by steep mountain fronts and intervening ~~push-ups; all~~structural highs. All of these morphotectonic features of the greater Marmara region are characterized by active Quaternary deformation process (Yildirim and Tüysüz, 2017). To the west of the Almacik Block, a transpressional push-up ridge, the NAFZ splits into three main strands (Fig. 1b; Armijo et al., 1999, 2002): the northern, middle, and southern branches. The northern branch traverses the Sea of Marmara and forms the N70°E striking Main Marmara Fault (MMF; Le Pichon et al., 2001; 2003). The approximately E-W-striking middle branch passes through the Armutlu Peninsula and continues along the southern coast of the Marmara Sea; this branch changes strike to NE-SW in the southern part of the Kapıdağ Peninsula (Yaltırak and Alpar, 2002; Kurtuluş and Canbay, 2007). The southern branch traverses the Biga Peninsula, the region to the south of the southern margin of the Marmara Sea.

The Marmara Sea is an E-W elongated transtensional basin with up to 1300 m water depth along its axial part; it is surrounded by onshore domains at about 600 m average elevation (Fig. 1c). The deepest part of the basin is the North Marmara Trough (NMT: Laigle et al., 2008; Bécel et al~~.~~., 2009), which hosts three main sedimentary basins along the NAFZ. These include the Çınarcık, Central, and Tekirdağ basins. These depocentres are separated from each other by the shallower Central High (East) and the Western High (West), respectively. In the deep parts of the basin protracted subsidence has resulted in the accumulation of more than 5 km of Pliocene–Holocene sediments (Le Pichon et al. 2001; 2003; 2015; Armijo et al. 2002; Parke et al. 2002; Carton et al., 2007; Laigle et al., 2008; Bécel et al. 2009; 2010; Bayrakci et al., 2013).

The region of the Marmara Sea is an integral part of the NAFZ, which ~~began~~has begun its activity in the east approximately 13 to 11 Ma ago (Şengör et al., 2005). Although different models and timing constraints for the onset of basin formation in the Marmara Sea have been presented in the context of the evolution of the NAFZ and the Aegean region (e.g., Armijo et al., 1999; Ünay et al., 2001; Yaltırak, 2002; Şengör et al., 2005; Le Pichon et al., 2014; 2015), offset geological marker horizons, ~~displace~~displaced structures, and paleontological data point to a transtensional origin during the propagation and sustained movement of the NAFZ with displacement and block rotations after the Zanclean transgression~~.~~ in the early Pliocene. Such a geodynamic scenario of transtensional dextral strike-slip faulting is compatible with space-geodetic data, the pattern of seismicity and geomorphic indicators in the landscape (Reilinger et al., 1997; 2006; Barka and Kadinsky-Cade, 1988; Bürgmann et al., 2002; Pucci et al., 2006; Akbayram et al., 2016; Yildirim and Tüysüz, 2017).

In contrast, based on GPS velocity data and surface geological observations, there are also arguments that the kinematics of the MMF correspond to a pure right-lateral strike-slip with the exception of the Çınarcık Basin area that the bend of the Princes Islands segment causes a transtensional setting (e.g. Le Pichon et al., 2003; 2015).

## 2. Method and model setup

Like for the earlier 3D model (Hergert and Heidbach, 2010), our study area extends from 40.25° N–27.25° E to 41.15° N–30.20° E and is projected as a rectangular shape in WGS84 UTM Zone 35N with a dimension of 250-by-100 km (Fig. 1c). It covers the Sea of Marmara and the adjacent onshore areas, as well as the city of Istanbul and the Bosporus.

The principal approach used for this study is crustal-scale 3D gravity forward modelling to assess the density configuration of different structural units. In this methodology, the gravity response of a model is calculated and compared with the observed gravity field. The model is iteratively modified to find the best–fit with observations. Since the solution is not unique in gravity modelling, it is required to reduce the number of free parameters by integrating other available geophysical and/or geological data as additional constraints. In the spirit of this philosophy, the workflow adopted in this study consists in: (1) setting up an initial density model (Fig. 2 and 3) – in our case based on the previous studies (Hergert and Heidbach, 2010; 2011; Hergert et al., 2011); (2) calculating the gravity response of this initial model and analysing the misfit (gravity residual) between modelled and observed gravity; (3) modifying the initial model by introducing additional density variations while integrating additional constraining data to obtain the density–geometry configuration that reproduces the observed gravity field best. In general, positive residual anomalies indicate that more mass is required in the model to fit the observed gravity field, whereas negative residuals imply that the mass in the model is too large in the domain of the misfit.

3D forward gravity modelling has been performed using the Interactive Gravity and Magnetic Application System–IGMAS+ (Transinsight GmbH©; Schmidt et al, 2011). In IGMAS+, the gravity response of a 3D structural and density model is calculated and compared with the observed gravity field over the model area. Therefore, the model has to be defined in terms of the geometric configuration of its individual structural units. In addition to geometry, information on the densities needs to be assigned to the different units of the model to calculate the gravity response. The chosen parameter combinations for the different models studied are detailed in Sect. 4. IGMAS+ provides the density-geometry configuration in the form of triangulated polyhedrons over the 3D model domain. These polyhedrons are spanned between 2D vertical working sections where the model can be interactively modified (Schmidt et al., 2011). For this study, a lateral resolution of 2500 meter is considered that results in 100 North-South oriented working sections. Downward the ~~model extends~~models extend to a constant depth of 50 km b.s.l and the unit comprised between the Moho and the lower model boundary is considered as the uniform lithospheric mantle. To avoid lateral boundary effects, the models extend on all sides 370 km further than the study area.

Key horizons where major contrasts in density are expected are the air-water interface, the sediment–water interface, the interface separating sediments and crystalline crust and the crust–mantle boundary (Moho). These interfaces also are well imaged with seismic methods and can therefore easily be integrated. Internal heterogeneities within the crust, may not be

identified by seismic methods or only locally along individual profiles. This is where 3D gravity modelling can be used in addition to translate velocities to densities first along the seismic section and use density modelling to close the gaps in between. This strategy together with the three-dimensionality of the calculation strongly reduces the non-uniqueness of gravity modelling as densities need to be in certain ranges for different rock types and density anomalies at different depths produce gravity effects of different wavelengths (e.g. Schmidt et al., 2011; Maystrenko et al., 2013; Sippel et al., 2013; Maystrenko and Scheck-Wenderoth, 2013).

To assess the density variations in the deeper crust of the Marmara Sea region, we calculate the gravity response for models of increasing complexity concerning their 3D structural and density configuration: (1) the initial model with homogeneous crust below the sediments, (2) a more differentiated model integrating additional seismic observations for the different crustal levels below the sediments, and (3) a series of final best–fit ~~model~~models in which the remaining residual anomaly is minimized by implementing additional density-geometry changes in the crust but respecting the seismic data. As two different gravity datasets are available, we calculate the difference between model response and observed gravity for both datasets.

Throughout the modelling procedure, the uppermost surface, the bathymetry (Fig. 1c), the top-basement depth (Fig. 2a) and the depth to the Moho discontinuity (Fig. 2b) are kept fixed as defined in the initial model since the geometries of these interfaces are well-constrained by geological and geophysical data. In all tested models an average density of 1025 $kg.m^{-3}$ was assumed for seawater, and a homogeneous density of 3300 $kg.m^{-3}$ is assigned to the mantle below the Moho. For all gravity models presented, we define the uppermost surface of the model as the onshore topography and as the sea level offshore. Accordingly, the thickness between sea level and bathymetry (Fig. 1c) corresponds to the column of seawater (Fig. 3a) which attains largest values in the Tekirdağ, Central, and Çınarcık basins.

## 3. Input data

The database for this study includes topography-bathymetry data, geometrical and density information from a previous 3D structural model, seismic observations, and ~~satellite~~different sets of published free-air gravity data including shipboard gravity dataset.

### 3.1. Topography and bathymetry

The topography–bathymetry (Fig. 1c) was exported from 1 Arc-Minute Global Relief Model (ETOPO1; Amante and Eakins, 2009). This dataset, over the study area, integrates the 30 arc-second grid obtained from NASA's Shuttle Radar Topography Mission (SRTM) and a bathymetry dataset (MediMap Group, 2005) with 1 km resolution. In addition, to increase the bathymetry resolution within the North Marmara Trough, high-resolution multibeam (EM300) acquired bathymetry (Le Pichon et al., 2001) is integrated into the model (Fig. S1 in the Supplement).

Figure 1c illustrates that the present-day Marmara Sea is surrounded by up to 1500 m high regions. The configuration of the present-day sea floor shows that the Marmara Sea is structured into the three main depocentres of the Tekirdağ Basin, the

Central Basin, and the Çınarcık Basin where the water depth reaches up to 1300 m. While the axis of the Central Basin is aligned along the MMF, the Çınarcık Basin and the Tekirdağ Basin extend only south and mostly north of the MMF, respectively. The MMF bends along the northern boundary of the Çınarcık Basin, at the Tuzla Bend, from an E-W directed strike (East of the Marmara Sea) to an ESE-WNW strike direction at the north-western margin of the Çınarcık Basin before it resumes the E-W strike direction at the Istanbul Bend. The segment of the MMF between the two bends is the Princes Islands Segment. Farther in the West of the Marmara Sea, at the Ganos Bend, the MMF once more changes strike direction from E-W to ENE-WSW. There, the MMF exits the Sea of Marmara and creates the Ganos Fault segment of the NAFZ.

### 3.2. Initial model

The 3D structural model (Fig. 3: Hergert and Heidbach, 2010; Hergert et al., 2011), considered to be the initial model for our study, differentiates three main horizons: (1) the topography–bathymetry (Fig. 1c), (2) a top-basement surface (Fig. 2a), and (3) the Moho discontinuity (Fig. 2b). In their study, Hergert and Heidbach (2010), modeled the top-basement geometry based on seismic observations (Parke et al., 2002; Carton et al., 2007; Laigle et al., 2008; Bécel et al., 2009; 2010) and other geophysical and geological data such as 3D seismic tomography (Bayrakci, 2009), well data (Ergün and Özel, 1995; Elmas, 2003) and geological maps (Elmas and Yigitbas, 2001). This surface, however, has been interpreted by others as the top of a Cretaceous limestone that is pre-kinematic with respect to the opening of the Sea of Marmara (Ergün and Özel, 1995; Parke et al., 2002; Le Pichon et al., 2014). Hergert and Heidbach (2010) derived the thickness of the sediments of the Marmara Sea as the difference between bathymetry-topography and top-basement. Accordingly, their "basement" delineates the base of the sediments and not the crystalline basement. First deep seismic surveys in the Sea of Marmara (Fig. 4: Laigle et al., 2008; Bécel et al., 2009) indicate that this basement is a pre-kinematic basement with respect to the opening of the Marmara Sea. Accordingly, Laigle et al. (2008), suggests the term of "syn-kinematic" infill for the sediments above the pre-kinematic basement. We, therefore, regard these sediments as the "syn-kinematic sediments" and refer to top-basement of the initial model as the "base syn-kinematic sediments" in the following.

The syn-kinematic sediments in our model represent the deposits related to the opening of the Marmara Sea and are interpreted to be mainly Pliocene–Quaternary infill (Laigle et al., 2008; Bécel et al., 2010; Bayrakci et al., 2013; Le Pichon et al., 2015). Accordingly, they are mostly missing in the domains outside the Marmara Sea in response to their syn-kinematic origin. They are characterized by normal fault-bounded initial synrift graben fills overlain by post-rift deposits overstepping the initial graben-like sub-basins. The full nature of the mechanical conditions for the Marmara Sea initiation are less clear. It is even partly still debated if the initiation of the Marmara Sea and the propagation of the Main Marmara Fault coincide in time. There are two competing hypotheses: (1) The Marmara Sea opened in extension, which weakened the lithosphere such that the North Anatolian Fault propagated along the weakened domains (e.g. Le Pichon et al., 2001; 2015) and (2) the releasing bend of the already propagated North Anatolian Fault or a dextral step-over between the Main Marmara Fault and the southern Fault favored local transtension resulting in the formation of the Marmara Sea as a pull apart basin (e.g. Armijo et al., 2002; 2005). However, seismic information proves that there is a clear change in the tectonic regime with the opening of the Marmara Sea

(Fig. 4: Laigle et al., 2008; Bécel et al., 2009; 2010, Bayrakci et al., 2013). The thickness between the topography–bathymetry and the base syn-kinematic sediments represents the syn-kinematic sediment fill (Fig. 3b). This thickness is on average about 2.5 km over the Marmara Sea area ~~and the unit is missing outside the Marmara Sea in response to its syn-kinematic origin.~~. Two thickness maxima indicate localized subsidence and sediment accumulation, one aligned along the MMF where the syn-kinematic sediments are more than 5.2 km thick below the present-day Central Basin and southeastern part of the Tekirdağ Basin, and the second maximum of up to 5 km below the Çınarcık Basin limited northward by the MMF.

The depth to the Moho interface in the initial model (Fig. 2b) has been obtained by interpolating between various seismic data covering a larger area than the model area (Hergert et al., 2011, Supporting Information, Fig. S1). To constrain the Moho depth to the model area, Hergert et al. (2011) applied a Gauss filter to adjust the local variation of the Moho depth. The Moho is distinctly shallower below the Marmara Sea than below the surrounding onshore areas and shows updoming to a depth of 27 km below the basin. Along the basin margins, the Moho is about 30 km deep and descends eastwards to more than 35 km depth beneath Anatolia.

### 3.3. Geophysical data

~~The~~The seismic observations considered for this study, in addition to those taken into account in the initial model, include P-wave velocity profiles from an offshore-onshore reflection-refraction survey (Bécel et al., 2009) and from a 3D seismic tomography study focused on the sediment-basement configuration of the North Marmara trough (Bayrakci et al., 2013). Both studies are based on the SEISMARMARA-Leg1 seismic survey (Hirn and Singh, 2001), and the locations of the related profiles in the model area are shown in Fig. 4a. Three-dimensional seismic tomography modelling in the North Marmara trough (Bayrakci et al., 2013) indicates that the P-wave velocities vary between 1.8 and 4.2 km.s$^{-1}$ within the syn-kinematic sediments. Bayrakci et al. (2013) derive the top of the crystalline basement as an iso-velocity surface with a P-wave velocity of 5.2 km.s$^{-1}$. In addition, relying on wide-angle reflection-refraction modelling, Bécel et al. (2009) interpreted a refractor below the base syn-kinematic sediments with a P-wave velocity close to 5.7 km.s$^{-1}$ as the top of the crystalline basement. These seismic studies suggest that the crust beneath the syn-kinematic sediments is not homogeneous as assumed in the initial model, but that there is a unit of pre-kinematic sediments beneath the syn-kinematic sediments with an average P-wave velocity of 4.7 km.s$^{-1}$ above the crystalline crust (Fig. 4). The pre-kinematic sediments encompass all deposits that have accumulated before the Marmara Sea opening. In the realm of the Marmara Sea, based on borehole observations, these deposits are separated from the syn-kinematic sediments by a diachronous unconformity that cuts units of variable age reaching from Early Cenozoic in the Upper Miocene to uppermost Cretaceous (Le Pichon et al., 2014). The pre-kinematic sediments are thinned in response to the extension/transtension related to the Marmara Sea opening that is most pronounced in the North Marmara Trough. Onshore, surface geological observations (Ergün and Özel, 1995; Genç, 1998; Turgut and Eseller, 2000; Yaltırak, 2002; Le Pichon et al., 2014) mapped Eocene–Oligocene sediments at the north-western and southern margins of the Marmara Sea that might be related to the missing units below the observed unconformity within the basin.

Furthermore, Bécel et al. (2009) interpreted a reflective horizon with a P-wave velocity of 6.7 km.s$^{-1}$ and largely parallel to the Moho topography as the top lower crystalline crust (Fig. 4b and 4c). Moreover, multichannel seismic reflection data collected in the southwestern part of the Central Basin and in the northeastern part of Marmara Island, documented a 43 km long low-angle dipping reflector interpreted as a normal detachment fault cutting through the upper crystalline crust down to the lower crust (Fig. 4c and 4e: Laigle et al., 2008; Bécel et al., 2009). In brief, within the upper crystalline crust, the P-wave velocity varies between 5.7 km.s$^{-1}$ at the top of the crystalline basement to 6.3 km.s$^{-1}$ above the top of the lower crystalline crust. Lateral velocity variations (~ 0.3 km.s$^{-1}$) are also observed surrounding the detachment fault in the upper crystalline crust.

The first set of gravity observations considered in this study are based on EIGEN-6C4 (Förste et al., 2014). This dataset is a combined global gravity field model up to degree and order 2190 correlating satellite observations (LAGEOS, GRACE, GOCE) and surface data (DTU 2'x2' global gravity anomaly grid). We used the free-air gravity anomaly, downloaded with the resolution of ETOPO1 (1 Arc-Minute), from the International Centre for Global Earth Models–ICGEM (Barthelmes et al., 2016~~).~~; Ince et al., 2019). The free-air anomaly map of the study area (Fig. ~~4a~~5a) displays generally low gravity values (±20 mGal) over the basin area indicating that the basin is largely isostatically compensated. An exception is a pronounced negative anomaly with values as low as -80 mGal in the northwestern segment of the Marmara Sea around the NAFZ. Comparing the bathymetry (Fig. 1c) with the free-air gravity anomaly map, it is evident that this negative anomaly is not related to a larger basin depth as bathymetry is rather uniform along the entire axial part of the basin. Likewise, the basement of the syn-kinematic sediments (Fig. 2a) is in the same range in both sub-basins. Accordingly, the negative anomaly is not due to thickness variations of the young sediments or water depth. Apart from the onshore area next to this negative anomaly, the Marmara Sea basin is surrounded by a chain of positive free-air gravity anomalies in a range of +70 to +120 mGal that largely correlate with high topographic elevations. ~~In summary, it can be stated that apart from the local negative anomaly domain~~

The second gravity dataset used in this study is a combined satellite (TOPEX) and marine ship gravity measurements (Fig. 5b: data from Kende et al., 2017). We refer to this dataset as "Improved–TOPEX". The satellite dataset is based on a marine gravity model from CryoSat-2 and Jason-1 with the horizontal resolution of 2500 meter and ~1.7 mGal of gravity accuracy over the Marmara Sea and Earth Gravitational Model 2008 over the onshore areas (EGM 2008: Pavlis et al., 2012; Sandwell et al., 2013; 2014). The shipboard gravity is from the Marsite Cruise survey in 2014 with ~1 meter of horizontal resolution. Alike the gravity observations from EIGEN-6C4, this combined gravity dataset shows mostly low gravity values (±20 mGal) over the sea of Marmara and a chain of large gravity values (+70 to +120 mGal) over the onshore domain apart from the northwestern part of the model. Along the MMF, there are local negative gravity values as low as -80, -70, and -50 spatially correlating with the sub basins of Central, Çınarcık and Tekirdağ, respectively.

The overall difference between these two datasets is a few mGals (±10 mGal), however, EIGEN-6C4 shows higher local gravity values up to 65 mGal at the southern part of the Princes Islands Segment and up to 50 mGals at the southern part of the Ganos Bend (Fig. 5c). As shown by Kende et al. (2017), the satellite gravity dataset of TOPEX has a good consistency with the processed Marsite shipboard gravity data, therefore, this discrepancy is due to the different satellite gravity datasets

of TOPEX and EIGEN-6C4. In summary and considering the discrepancy between the two datasets, it can be stated that apart from the local negative anomaly domains, the syn-kinematic sediments need to be isostatically balanced in the crust, given that the Moho topography is varying on a far longer wavelength below the basin.

~~The seismic observations considered for this study, in addition to those taken into account in the initial model, include P-wave velocity profiles from an offshore-onshore reflection-refraction survey (Bécel et al., 2009) and from a 3D seismic tomography study focused on the sediment-basement configuration of the North Marmara trough (Bayrakci et al., 2013). Both studies are based on the SEISMARMARA-Leg1 seismic survey (Hirn and Singh, 2001), and the location of the related profiles in the model area are shown in Fig. 4b. Based on 3D seismic tomography modelling in the North Marmara trough (Bayrakci et al., 2013) indicates that the P-wave velocities vary between 1.8 and 4.2 km.s$^{-1}$ within the syn-kinematic sediments, and derives the top of the crystalline basement as an iso-velocity surface with a P-wave velocity of 5.2 km.s$^{-1}$. In addition, relying on wide-angle reflection-refraction modelling, Bécel et al. (2009) interpreted a refractor below the base syn-kinematic sediments with a P-wave velocity close to 5.7 km.s$^{-1}$ as the top of the crystalline basement. Furthermore, they interpreted a reflective horizon with a P-wave velocity of 6.7 km.s$^{-1}$ and largely parallel to the Moho topography as the top lower crystalline crust. Moreover, multichannel seismic reflection data collected in the southwestern part of the Central Basin and in the northeastern part of Marmara Island, documented a 43 km long low-angle dipping reflector interpreted as a normal detachment fault cutting through the upper crystalline crust down to the lower crust (Bécel et al., 2009).~~

~~In brief, these seismic studies suggest that the crust beneath the syn-kinematic sediments is not homogeneous as assumed in the initial model, but that there is a unit of pre-kinematic sediments beneath the syn-kinematic sediments with an average P-wave velocity of 4.7 km.s$^{-1}$ above the crystalline crust. Within the upper crystalline crust, the P-wave velocity varies between 5.7 km.s$^{-1}$ at the top of the crystalline basement to 6.3 km.s$^{-1}$ above the top of the lower crystalline crust. Lateral velocity variations (~ 0.3 km.s$^{-1}$) are also observed surrounding the detachment fault in the upper crystalline crust.~~

## 4. Results

In addition to the initial structural model with a homogeneous crustal layer below the syn-kinematic sediments (Fig. 3), relying on seismic profiles (Fig. ~~4b~~4), we modified the structural model ~~that differentiate~~differentiating three crustal layers (Fig. ~~5).~~ 6). Considering the two different datasets (EIGEN-6C4 and Improved–TOPEX) and the non-uniqueness in potential field modelling, a range of possible configurations were tested of which we present three possible best-fit models obtained from the 3D forward gravity modelling. These results are summarized in Table 1. The gravity response of these ~~two different~~ 3D structural density models and their corresponding residual gravity anomaly for each of the two gravity datasets are shown in Fig. ~~6 and~~ 7 and 8, respectively. ~~Here, we show these models and present a best-fit model obtained from the 3D forward gravity modelling (Fig. 8, 9, 10). These results are summarized in Table 1.~~

### 4.1. Initial model

The initial model (Hergert and Heidbach, 2010; Hergert et al., 2011) resolves only the three structural units: water, syn-kinematic sediments, and a homogeneous crust (Fig. 3). Hergert et al. (2011) considered a depth-dependent density gradient based on seismic velocities for the sediments and crust. The gradient profile varies between 1700 to 2300 kg.m$^{-3}$ within the syn-kinematic sediments, between 2500 to 2700 kg.m$^{-3}$ for the first 20 % of the crust, and from 2700 to 3000 kg.m$^{-3}$ for the lower parts of the crust. According to this profile, we derived thickness-weighted average densities of 2000 and 2800 kg.m$^{-3}$ for the syn-kinematic sediments and the crust, respectively.

The calculated gravity response of the initial model (Fig. ~~6a~~7a) indicates a significant misfit with respect to the observed gravity of EIGEN-6C4 (Fig. ~~4a~~5a). In ~~the onshore domain and~~ the eastern part of the model, the misfit between observed and modelled gravity is rather small and ranges between ±20 mGal (Fig. ~~7a~~8a). Furthermore, within the offshore domain, along the MMF, there are two local positive residual gravity anomalies with more than +90 mGal ~~(~~("A" and "B" in Fig. ~~7a~~8a). These positive anomalies indicate mass deficits in the model and spatially correlate with the bends along the MMF: one occurs in the southern part of the Princes Islands Segment, between the Tuzla Bend and the Istanbul Bend, and the other one is present south of the Ganos Bend. There is also a local short-wavelength positive residual anomaly, reaching values higher than +60 mGal at the location of the Imralı Basin ~~(~~("C" in Fig. ~~7a~~8a). In addition, a pronounced West-East oriented continuous negative residual anomaly of around -50 mGal is detected adjacent to the southern coastline.

The gravity response of the initial model shows a better fit with the observed gravity of Improved–TOPEX compared to EIGEN-6C4 (Fig. 8b). In the onshore domain, the residual anomalies are very similar to the residual anomalies for the EIGEN-6C4 dataset. Offshore, a distinct West-East oriented continuous positive residual anomaly of around +40 mGal is noticeable along the MMF for the Improved–TOPEX dataset. In addition, two local positive residual gravity anomalies of "A" and "B" (Fig. 8a) are evident up to +60 mGal for the Improved–TOPEX dataset. The short-wavelength positive residual anomaly of "C" previously observed across the Imralı Basin (Fig. 8a) is also evident for the Improved–TOPEX dataset but with a lower value of residual gravity up to +40 mGal.

Overall, these ~~results~~residuals for both gravity datasets indicate that the long-wavelength gravity field is reproduced by the initial model and that the Moho topography (Fig. 2b) is consistent with observed gravity. However, the large residual anomalies of a few tens of km in diameter indicate the presence of crustal density heterogeneities causing gravity anomalies of smaller wavelengths, i.e. shallower depth.

### 4.2. Differentiated crust

In addition to this indication of density heterogeneities in the crust from gravity, also seismic observations (e.g. Laigle et al., 2008; Bécel et al., 2009; 2010; Bayrakci, 2009; Bayrakci et al., 2013) point to crustal heterogeneity expressed as distinct lateral and vertical variations in seismic velocity~~.~~ (Fig. 4). To integrate the outcomes of the seismic studies, we ~~vertically~~ differentiate

the crust in ~~a~~the next step into three units: (1) a unit of pre-kinematic sediments, (2) a unit of upper crystalline crust, and (3) a lower crystalline crustal unit.

#### 4.2.1. Pre-kinematic sediments

In the initial model (Hergert and Heidbach, 2010; Hergert et al., 2011), the upper limit of the crust below the syn-kinematic sediments (their "top-basement") was mainly defined as pre-kinematic Cretaceous limestone (Ergün and Özel, 1995; Parke et al., 2002; Le Pichon et al., 2014): a surface corresponding to an increase of P-wave velocity to values larger than 4.5 km.s$^{-1}$. Furthermore, Bécel et al. (2009) interpreted a top crystalline basement as a surface where P-wave velocity increases to values above 5.7 km.s$^{-1}$ based on seismic imaging. In addition, Bayrakci et al. (2013) derived the top of the crystalline crust at an iso-velocity surface of 5.2 km.s$^{-1}$ based on a 3D P-wave tomography model beneath the North Marmara Trough. These seismic observations justify the differentiation of an additional unit of pre-kinematic sediments. Accordingly, we implement a unit the upper limit of which corresponds to the top of the pre-kinematic Cretaceous limestone (=base syn-kinematic sediments in the initial model) while its base corresponds to the top crystalline basement (Fig. ~~5).~~ 6).

The top crystalline crust topography proposed by Bécel et al. (2009) and by Bayrakci et al. (2013) is similar, and the depth difference between the surfaces presented in the two studies is ~~mainly~~mostly less than 2 km~~.~~ (Fig 4c). Therefore, we derive the geometry of the top crystalline basement for the gravity test applying a convergent interpolation between the seismic profiles (Fig. ~~4b~~4) of Bayrakci et al. (2013) and of Bécel et al. (2009).

As the newly implemented pre-kinematic sedimentary unit represents the Pre-Marmara Sea deposits, it is mostly absent in the realm of the present-day Marmara Sea (Fig. ~~5a~~6a). Its thickness displays maxima of up to ~~6.5~~7.2 km along the north-western and southern margins of the present-day Marmara Sea and significantly decreases eastwards to less than 1.5 km.

Bayrakci et al. (2013) showed that the average velocity of the pre-kinematic sediments is around 4.7 km.s$^{-1}$. To convert the velocity information for this unit into density, we use an empirical equation (Eq. 1) which is a polynomial regression to the Nafe–Drake Curve valid for P-wave velocities between 1.5 to 8.5 km.s$^{-1}$ (Fig. S2 in the Supplement: Brocher, 2005 after Ludwig et al., 1970). Correspondingly, an average density of 2490 kg.m$^{-3}$ has been assigned to the pre-kinematic sediments, considering an average P-wave velocity of 4.7 km.s$^{-1}$.

$$\rho\ (g.cm^{-3}) = 1.6612V_p - 0.4721V_p^2 + 0.0671V_p^3 - 0.0043V_p^4 + 0.000106V_p^5 \qquad \text{(Eq. 1)}$$

#### 4.2.2. Crystalline crust

Apart from the unit of pre-kinematic sediments, the P-wave velocity model of Bécel et al. (2009) differentiates an additional crustal interface across which P-wave velocities increase from values of around 6.2 km.s$^{-1}$ above the interface to values higher than 6.7 km.s$^{-1}$ below. They interpreted this interface as the top of the lower crystalline crust. Consequently, we applied a convergent interpolation between the seismic profiles (Fig. ~~4b~~4) of Bécel et al. (2009) to derive the top lower crystalline crust implemented into the next model. Eventually, we considered the thickness between the top crystalline basement and the top of

the lower crystalline crust as the upper crystalline crustal unit. Its thickness distribution (Fig. ~~5b~~6b) shows pronounced thickness minima below the thickness maxima of the syn-kinematic sediments, where the upper crystalline crust is less than 12 km thick. In contrast, the upper crystalline crust is up to 23 km thick below the south-western margin of the present-day Marmara Sea and reaches more than ~~26~~25 km in thickness along the eastern margin.

Below the upper crystalline crust, a lower crystalline crustal unit ~~follows, bounded on its top by the top lower crystalline crust and at~~is modelled, bounded its base by the Moho discontinuity. It is characterized by an almost uniform thickness distribution (Fig. ~~5c~~6c) of around 10 km across the ~~model area~~Sea of Marmara. In the north-western corner of the model area, where the Moho surface (Fig. 2b) descends, the thickness of the modelled lower crystalline crust reaches its maximum of up to ~~15~~14 km. In contrast, ~~the lower crystalline crust~~ this unit thins to less than ~~6~~5 km below the south-western ~~margin~~and north-eastern margins of the present-day Marmara Sea, where the upper crystalline crust thickens to 23 ~~km. Two other local areas where the lower crystalline crust has a reduced thickness (less than 7 km) are aligned in a N-S direction in the eastern central part of the study area: one~~and 25 km, respectively. Offshore, adjacent to ~~the Bosporus in the North, and a second one south~~ of Armutlu Peninsula, the lower crystalline crust has an increased thickness (up to 13 km) correlating with the upper crustal thinning to around 12 km.

Throughout the upper crystalline crustal unit, seismic velocities increase with depth from 5.7 km.s$^{-1}$ to 6.3 km.s$^{-1}$ (Bécel et al., 2009). Therefore, we considered 6 km.s$^{-1}$ as the average P-wave velocity of the upper crystalline crust. P-wave velocities for the lower crystalline crust show less variation, thus, 6.7 km.s$^{-1}$ has been adopted as the average P-wave velocity within the lower crystalline crust. The density for both crystalline crustal layers, are calculated respecting the P-wave velocities (Eq. 1) as 2720 kg.m$^{-3}$ and 2890 kg.m$^{-3}$ for the upper and lower crystalline crust, respectively.

The gravity calculated for this refined model shows a better fit with the observed gravity ~~field~~datasets in comparison to the initial model (Fig. ~~7a and 7b~~8). Nevertheless, regarding the EIGEN-6C4 dataset, the three local large positive residual gravity anomalies observed for the initial model ~~(~~(“A~~,~~”, “B~~;~~”, and “C” in Fig. ~~7a~~8a) are still ~~evidently~~evident indicating that the implemented subdivision of the crust alone is insufficient~~. The short-wavelength positive anomaly at location C could be interpreted as a local lack of mass within the modelled sedimentary fill of the Imralı Basin. However, the~~ (Fig. 8c). The wavelength of the two other positive residual anomalies at “A” and “B” is too large to be caused by a high-density feature at the sedimentary fill level but too small to be a result of density heterogeneities in the mantle. Thus, we concluded that these misfits are most likely related to high-density bodies within the crystalline crust. The short-wavelength positive anomaly at location “C” could be interpreted as a local lack of mass within the modelled sedimentary fill of the Imralı Basin.

In contrast, considering the Improved–TOPEX dataset, implementing the pre-kinematic sediments and two crystalline crustal units instead of a uniform crustal unit successfully compensate the local positive residuals of “C” over the Imralı Basin as well as the West-East oriented continuous positive residual anomaly along the MMF (Fig. 8d). However, the residual map still shows values of negative anomalies down to -60 mGal across the Marmara Island, in the north east of the Kapidag Peninsula (offshore), and over the Armutlu Peninsula (D, E, and F in Fig. 8d). In addition, up to +50 mGal of positive residual anomalies are detected in the north-eastern margin of the Marmara Sea and across the Tekirdağ Basin (G and H in Fig. 8d).

#### 4.2.3. Best-fit ~~Model~~models

To overcome ~~these~~the remaining misfits between modelled and observed gravity ~~(A and B in Fig. 7a),~~, we ~~applied~~incorporated additional crustal density heterogeneities during forward gravity modelling ~~to test different structural density configurations within the crust.~~that we tested with respect to both gravity datasets. The gravity response of the best-~~-~~fit ~~model is~~models and their corresponding residuals are shown in ~~Fig. 6c and the residual in Fig.~~ Figure. 7c~~.~~-e and Figure 8e-g, respectively. Over most of the model area, the residual gravity anomaly (Fig. ~~7c~~8e-g) shows differences between modelled and observed gravity datasets of ±20 mGal. Achieving this fit required the implementation of two dome-shaped high-density bodies of considerable dimension in the crystalline crust. ~~In the best-fit model, these bodies have an average density of 3050~~Considering the differences between the two alternative gravity datasets (Fig. 5) and non-uniqueness of the gravity method, several configurations of these high-density bodies are plausible that differ in size or density. Here, we present three possible endmembers of the high-density bodies respecting both gravity datasets: one model for EIGEN-6C4 (Model-I) and two models for Improved–TOPEX (Model-II and Model-III).

##### 4.2.3.1 Best-fit model to EIGEN-6C4 (Model-I)

In this best-fit model high-density bodies have an average density of 3150 kg.m$^{-3}$, being thus denser than the lower crystalline crust (average density 2890 kg.m$^{-3}$), but less dense than the Mantle (3300 kg.m$^{-3}$). They extend from the Moho upward, cutting through the lower crystalline crust, and reaching into the upper crystalline crust as shallow as ~~the top crystalline basement at about 4~~~5 km depth. Accordingly, the high-density bodies attain thicknesses of up to ~~26~~25 km (Fig. ~~8~~9 and ~~9~~10).

The position of these high-density bodies spatially correlates with the domains where the MMF bends (Fig. 9 and ~~10~~11). At the western margin of the Marmara Sea and below the Ganos Bend, the high-density body cuts the lower crystalline crust at a depth of around ~~21~~22 km b.s.l and continues through the upper crystalline crust. The shallower part of this body (less than ~~5~~6 km b.s.l) is located directly ~~south~~east of the Ganos Bend, where the MMF changes its strike direction from E-W to ENE-WSW ~~(Fig. 10).~~. Likewise, the second high-density body is modelled beneath the Princes Islands Segment at the eastern margin of the Marmara Sea, and the top of the body is located at a depth of ~~less than~~around 5 km b.s.l (Fig. ~~10~~9 and 11).

By introducing the two high-density bodies into the structural model, eventually, the thickness distribution of the upper and lower crystalline crust has changed ~~(Fig. 9)~~ below the Çınarcık and Tekirdağ basins, where the high-density bodies largely replace the crystalline crustal units~~.~~ (Fig. S3 in the Supplement). Over the rest of the model area, the thickness distribution of the crystalline crustal units is similar to the one in the model explained in Sect. 4.2.2. Remarkably, the long axis of the eastern high-density ~~bodies~~body follows the strike ~~directions~~direction of the ~~bent segments of the MMF~~Princes Islands segment (Fig. 9 and ~~10~~11). In addition, a spatial correlation is evident between the location of the two high-density bodies with the position of the young depo-centres of the Çınarcık and Tekirdağ basins as indicated by deepest present-day bathymetry and by thickness maxima of the syn-kinematic sediments (Fig. 1c and 3).

4.2.3.2 Best-fit models to Improved –TOPEX (Model-II and Model-III)

As shown earlier, the model with the differentiated crustal units (Fig. 6) already represents a good fit to Improved-TOPEX (Fig. 8d). Here, we quantify the influence of the high-density bodies with an average density of 3150 kg.m$^{-3}$ on the gravity response. The forward gravity modelling output indicates that the high-density bodies need to be smaller in size for the same average density value (Model-II). The corresponding misfit between Model-II and observed gravity of Improved–TOPEX shows that the positive residuals of "G" and "H" are considerably reduced as well as the continuous negative residuals at the southern margin of the Marmara Sea (Fig. 8f). Comparing with Model-I (the best-fit model to EIGEN-6C4), these high-density bodies can be modelled for the same location but with a smaller maximum thickness of ~16 km (Fig. 9, 10, 11).

As the second endmember solution for a best-fit model to Improved-TOPEX (Model-III), we test a configuration in which the geometry of the high-density bodies is identical to Model-I (the best-fit model to EIGEN-6C4). Therefore, the Model-III has a similar structural setting as Model-I. The results show that an average density of 2890 kg.m$^{-3}$, equivalent to the value assigned for the lower crust average density, would fit the gravity response of Model-III to Improved–TOPEX dataset best (Fig. 8g).

In summary, all three best-fit models indicate significant lateral density variation within the crystalline crust and require the presence of two dome-shaped high-density bodies that spatially correlating with the bends of the MMF with the density ranges of ~2890 to ~3150 kg.m$^{-3}$.

## 5. Interpretation and discussion of the best-fit ~~model~~models

The response of the best-fit gravity ~~model~~models (Fig. ~~6c~~7c-e) and ~~its~~their corresponding misfit (Fig. ~~7c~~8e-g) confirmed that the crust below the Marmara Sea is characterized by significant density heterogeneities. In summary, ~~the model predicting gravity best resolves~~these models resolve six ~~structural~~crustal units with different densities that ~~indicates~~indicate different lithological settings ~~(~~within the crust (Fig. 10 and Table 1).

The uppermost and youngest layer is the present-day water column (Fig. 3a) that is largest in the present-day sub-basins of the Marmara Sea and underlain by the unit of syn-kinematic sediments of the Marmara Sea (Fig. 3b). These syn-kinematic sediments are present ~~only~~mainly inside the Marmara Sea domain and their thickness distribution indicates a subsidence regime similar to the present-day one. The relationship between the individual sub-basins of the Marmara Sea and the course of the MMF are however different: The shape of the present-day Tekirdağ Basin is not evident in the thickness distribution of the syn-kinematic sediments, whereas the Central Basin along the MMF and the Çınarcık Basin are largely following their present-day counterparts. This indicates that the differentiation into the present-day Central and Çınarcık basins postdates the syn-kinematic phase of the Marmara Sea. The average density ~~and~~of 2000 kg.m$^{-3}$and the observed seismic velocities of 1800 to 4200 m.s$^{-1}$ (Bayrakci et al., 2013) indicate that this unit is mainly composed of poorly consolidated clastic deposits. There is, however, little information on their precise ages; suggested time intervals for the deposition of this unit range from Late Miocene to Holocene with a longer deposition portion of the unit assigned to the interval between Pliocene ~~to~~and Holocene times (Le Pichon et al., 2014; 2015).

The third modelled unit is characterized by an average density ~~(~~of 2490 kg.m$^{-3}$~~)~~ and by observed seismic velocities ~~(~~of 4200-5200 m.s$^{-1}$ (Fig. 4d and 4e: Laigle et al.,2008; Bayrakci et al., 2013) representative for sediments. At the same time, the unit is largely missing below the present-day Marmara Sea. We, therefore, interpret this unit as a Pre-Marmara Sea sedimentary unit above the top crystalline basement. The areas where the maximum thickness of more than 6 km are modelled for the pre-kinematic sediments (NW and S of the Sea of Marmara) coincide spatially with the location where Pre–Neogene rocks are present according to surface geology (Yaltırak, 2002). Other surface geological observations (Ergün and Özel, 1995; Genç, 1998; Turgut and Eseller, 2000; Le Pichon et al., 2014) also report the presence of Eocene–Oligocene sediments at the location where the maximum thickness of the pre-kinematic sediments unit is modelled.

The sedimentary units are underlain by the upper crystalline crust, which is thinned below both the Marmara Sea and the pre-kinematic sediments. This indicates that upper crustal thinning accompanied both phases of basin evolution. Both, the modelled average density and observed seismic velocities for the upper crystalline crust indicate that this unit is dominantly composed of felsic ~~metamorphic~~crystalline rocks. A comparison of the average density ~~(~~of 2720 kg.m$^{-3}$~~)~~ and average P-wave velocity ~~(6 km~~of 6000 m.s$^{-1}$ (Bécel et al., 2009) of the upper crystalline crust with a ~~compilation~~ velocity–density pairs derived from laboratory measurements (Christensen and Mooney, 1995) indicates a composition corresponding to phyllites and/or biotite gneisses.

Below the upper crystalline crust, the lower crystalline crust follows, the top of which is largely parallel to the Moho topography. The thickness of this unit (Fig. ~~5c~~6c) indicates no clear spatial relationship with the formation of both generations of pre- and syn-kinematic basins. Here, the modelled average density and observed seismic velocities are indicative for an intermediate to mafic composition. Combining the physical properties of the lower crystalline crust ($\rho$ = 2890 kg.m$^{-3}$ & $V_p$= ~~6.7 km~~6700 m.s$^{-1}$) and the property compilations of Christensen and Mooney (1995), the lithology of the lower crustal unit could be interpreted as diorite and/or granulite.

The sixth unit ~~resolved in the best-fit gravity model~~is the one with largest differences in density-geometry configuration based on the forward gravity modelling to the two alternative gravity datasets. For this unit, we predict three alternative lateral density configurations that all entail two dome-shaped high-density bodies within the crystalline crust: two models with an average density of 3150 kg.m$^{-3}$ (Model-I and Model-II) and one model with an average density of 2890 kg.m$^{-3}$ (Model-III).

### 5.1. High-density bodies of 3150 kg.m$^{-3}$ (Model-I and Model-II)

In the best-fit gravity model with respect to EIGEN-6C4 (Model-I), the sixth unit encompasses two high-density bodies rising from the Moho in a dome-shaped manner through both crystalline crustal layers~~, partly up to the top crystalline basement~~ (Fig. ~~8 and 9~~9a). For these bodies, a rather high density (~~3050~~3150 kg.m$^{-3}$) has to be assumed which indicates that they are of mafic composition. Considering the seismic velocity and density relationship (Eq. 1), a corresponding average P-wave velocity for such a high-density body with an average density would be around 7.~~27~~5–7.~~28~~6 km.s$^{-1}$. ~~This combination of physical properties would indicate gabbroic intrusive rock (Christensen and Mooney, 1995) as a possible lithological interpretation for~~

In contrast, the forward gravity modelling with respect to Improved–TOPEX (Model-II) predicts the sixth unit with the same average density value of 3150 kg.m$^{-3}$ to be smaller in size (Fig. 9b). In both solutions, the locations of the high-density bodies~~.~~ ~~Their locations~~ correlate spatially with the bent segments of the MMF (Fig. 9 and ~~10~~11) indicating that such a mafic composition in concert with their considerable thickness could result in greater strength compared to the surrounding felsic upper crust or the intermediate-mafic lower crust.

The mechanisms and timing of the emplacement of the high-density bodies are, however, difficult to determine. The modelled density indicates that the high-density bodies represent magmatic additions to the Marmara crust, potentially originating from larger depths that rose buoyantly into domains of local extension. Magnetic anomalies across the Sea of Marmara indicate positive anomalies along the MMF that may be interpreted as magnetic bodies along the fault (Ates et al., 1999; 2003; 2008). In particular, the locations of the high-density bodies beneath the Çınarcık Basin correlate spatially with the maximum positive magnetic anomaly (Ates et al. 2008) which indicates that some mafic lithology is present there below the non-magnetic sediments.

The spatial correlation between the position of the high-density bodies and the position of the eastern thickness maxima in the syn-kinematic sediments indicates that subsidence in the syn-kinematic basins at least partly took place in response to cooling of previously emplaced (magmatic) high-density bodies. This would imply that the emplacement of the high-density bodies predates the formation of the Marmara Sea sub-basins and the propagation of the MMF. To assess the possible contribution of thermal cooling to the subsidence history of the Marmara Sea, a detailed subsidence analysis with determination of the tectonic subsidence would be required.

As we do not have further evidence for a magmatic origin of the high density bodies, other possible interpretations of these domains may be considered. For example, these high density bodies could represent inherited structures of former deformation phases such as ophiolites along the intra-Pontide suture that has been mapped on land, but have not yet been explored offshore (Okay and Tüysüz, 1999; Robertson and Ustaömer, 2004; Le Pichon et al., 2014; Akbauram et al., 2016). The two different emplacement mechanisms would have opposing consequences for the propagation of the North Anatolian Fault. The magmatic origin would be consistent with crustal weakening in these domains, whereas the ophiolite origin would imply the opposite. In both cases, however, a local strength anomaly in these domains would be the consequence that could be related to the bending of the fault. Whatever the origin of these bodies, their mafic composition would imply that they represent domains of higher strength in the present-day setting.

### 5.2. High-density bodies of 2890 kg.m$^{-3}$ (Model-III)

In Model-III as the alternative best-fit model for the Improved–TOPEX gravity dataset, the sixth unit has been calculated identical to the geometry of Model-I (Fig. 9a) but with the average density of 2890 kg.m$^{-3}$ as similar to average density of the lower crust. This density value is consistent with the average density value of intermediate to mafic metamorphic rocks such as granulite (Christensen and Mooney, 1995). In this case, these two dome-shaped bodies may be interpreted as trapped

metamorphic rocks along the Intra-Pontide suture zone that spatially correlates with the MMF propagation (Şengör et al., 2005; Le Pichon et al., 2014; Akbauram et al., 2016).

Several studies of exhumed orogen related strike-slip faults indicate that dome-shaped metamorphic bodies of lower crust is a common phenomenon below transtensional pull-apart basins (Leloup et al., 1995; West and Hubbard, 1997; Jolivet et al., 2001; Labrousse et al., 2004; Corsini and Rolland, 2009;). Thus the high-density bodies could represent metamorphic core complexes exhumed in response to strike-slip deformation. Such exhumation has also been proposed from numerical modelling studies across strike-slip basins such as the Sea of Marmara or the Dead Sea (Sobolev et al., 2005; Le Pourhiet et al., 2012; 2014).

### 5.3. Comparison with published 3D density model

In a previous density modelling study, Kende et al. (2017) inverted the long-wavelength gravity signals to derive the Moho topography below the Marmara region using the same Improved–TOPEX gravity dataset that we used in our study. We also consider the same bathymetry and the same seismic dataset within the Marmara Sea as Kende et al. (2017). The main difference between their density modelling and ours consists in the applied gravity methods. In our approach we applied forward gravity modelling method while Kende et al. (2017) mainly used an inversion method to compensate the misfit between modelled and observed gravity. The second principal difference is that Kende at al. (2017) considered the Moho depth as the primary reason for the misfit. As mentioned earlier (4.1. Initial model), the depth to the Moho in our model (Fig. 2b) has been obtained based on various seismic data covering a larger area than the Marmara region (Hergert et al., 2011, Supporting Information, Fig. S1) and was kept fixed during the forward gravity modelling. In contrast, the Moho topography in Kende et al. (2017) was obtained by gravity inversion.

We have tested the full density model of Kende et al. (2017) and the results are presented as supplementary information (Fig. S4 and S5). The misfit between the previous model (Kende et al, 2017) and the observed gravity of EIGEN-6C4 (Fig. S5 in the Supplement) generally has the same characteristics as the misfit between our differentiated crust model (two sediments units / upper crust / lower crust) and EIGEN-6C4 observed gravity (Fig. 8c). This indicates that the two positive residual anomalies of “A” and “B” (Fig. 8) are not related to the sediment thickness. Specifically, it means that the local Moho uplifts in the model of Kende et al. (2017) would need to be much larger than 5 km to fit the calculated gravity if one considered the observed gravity datasets of EIGEN-6C4.

Comparing with their results, there are consistent findings in our study and the study of Kende et al. (2017). In particular, the latter also shows the need for deep compensation of the sedimentary fill, however, the authors propose to solve the problem with an uplift of the Moho in the domains of our lower crustal high-density bodies. In detail, assuming a laterally uniform density of the crystalline crust, they propose ~5 km local shallowing of the Moho. In other words, Moho uplifts in their model are also high-density bodies that are 5 km thick with a density of 3330 $kg.m^{-3}$ which is comparable to ~16 km thick high-density bodies with an average density of 3150 $kg.m^{-3}$ or ~25 km thick high-density bodies with an average density of 2890 $kg.m^{-3}$ in our models.

## 5.4. Model limitations

~~The modelled upper and lower crystalline crustal units are in consistency with seismic observations and velocity modelling (Laigle et al.,~~The modelled upper and lower crystalline crustal units are consistent with seismic observations and velocity modelling (Fig. 4 and Fig. 10: Laigle et al., 2008; Bécel et al., 2009; 2010; Bayrakci et al., 2013). In contrast, seismic studies did not report the presence of large high-velocity bodies that would coincide spatially with the modelled high-density bodies. There are only a few indications from seismic tomography (Bayrakci et al., 2013) discriminating a zone of high P-wave velocity (Vp > 6.5 km.s$^{-1}$) ~~beneath~~below the top crystalline basement beneath the Çınarcık Basin~~.~~ (Fig. 4). This high-velocity zone approximately correlates with the top of the high-density body in this area~~.~~ (Fig. 10). In addition, other tomography results (Yamamoto et al., 2017) indicate a zone of higher S-wave velocity and slightly higher P-wave velocity at about 20 km depth b.s.l, in the area where the western high-density body cuts the boundary between the upper and the lower crystalline crust.

## ~~5.1. Model limitations~~

The gravity ~~response~~responses of the best-fit ~~model presents~~models present a good fit (±20 mGal) over most of the model area. Nevertheless, there are still some negative residual gravity anomalies ~~where observed and modelled gravity differ by more than 70 mGal at~~ across the Marmara Island ~~(D,~~ in ~~Fig. 7c)~~the north east of the Kapidag Peninsula (offshore), and ~~by more than 50 mGal at~~over the Armutlu Peninsula ~~(~~("D", "E", and "F" in Fig. ~~7c). These~~8). The short-~~wavelength~~wavelengths of these negative residual anomalies indicate that shallow low-density features remain unresolved in the model.

~~The thickness distribution maps (Fig. 3, 5, and 9~~ Regarding the negative residuals anomaly at location "E", an interpretation remaining difficult due to the offshore location of the anomaly. In contrast, considering the surface geological observations might help to reveal the negative residual at the location of the Marmara Island and the Armutlu Peninsula. The thickness distribution maps (Fig. 3 and 6) show that Marmara Island is dominantly exposing rocks of the upper crystalline crust. More precisely, geological surface observations in this area (Aksoy 1995; 1996; Attanasio et al., 2008; Karacık et al., 2008; Ustaömer et al., 2009) differentiate three main rock types in outcrops: A Permian Marble unit in the North, an Eocene Granodiorite unit in the centre, and a Permian Metabasite in the South of Marmara Island. Considering the residual anomalies (Fig. ~~7c~~8), these three units have densities that are different from the average density assumed for the upper crystalline crust (2720 kg.m$^{-3}$). ~~This could explain the obtained misfit with the observed gravity in this region (D in Fig. 7c).~~ Our result of obtaining a negative residual indicates that the subsurface extent of rocks with densities lower than the assumed average for the upper crystalline crust is larger than that of the units with higher densities. In other words, the marbles would make a larger portion of the island's subsurface than the metabasites or granodiorites.

The negative residual anomaly at Armutlu Peninsula ~~(E~~("F" in Fig. ~~7c~~8) is found where the syn-kinematic sedimentary unit is absent (Fig. 3b), whereas a thickening of the pre-kinematic sediments is modelled there (Fig. ~~5a~~6a). Geological maps (Genç, 1998; Yaltırak, 2002; Akbayram et al., 2016) show that this area is mainly covered by Pre-Neogene basement, Miocene acid-intermediate volcanic rocks, and some Pliocene–Holocene clastic sediments. However, the model does not account for these

locally documented occurrence of syn-kinematic sediments (Pliocene–Holocene clastics) and of Miocene volcanic rocks in this domain, which overall could explain the negative residual anomaly.

### 5.~~2~~5. Implications

The gravity modelling demonstrates that considering a homogenous crystalline crust beneath the Sea of Marmara is not a valid assumption, but that rather a two-layered crystalline crust crosscut by two large local high-density ~~bodies is plausible. (~~3150 kg.m$^{-3}$) bodies is plausible~~The mechanisms and timing of the emplacement of the high-density bodies are, however, difficult to determine.~~ The modelled density indicates that the high-density bodies represent magmatic additions to the Marmara crust, potentially originating from larger depths and have buoyantly risen into domains of local extension. The spatial correlation between the position of the high-density bodies and the position of thickness maxima in the syn-kinematic sediments indicates that subsidence in the syn-kinematic basins at least partly took place in response to cooling of the previously emplaced (magmatic) high-density bodies. This would imply that the emplacement of the high-density bodies predates the formation of the Marmara Sea sub-basins and the propagation of the MMF. To assess the possible contribution of thermal cooling to the subsidence history of the Marmara Sea, a detailed subsidence analysis with determination of the tectonic subsidence would be required~~.

~~A second~~An interesting finding is the spatial correlation between the position of the high-density bodies and the bent segments of the MMF. If the high-density bodies represent high-strength domains of the Marmara Sea crust, it would cause local stress deviations influencing the fault propagation direction. The 3D view on the fault plane in relation to the high-density bodies position illustrate how the fault bends in these high-strength domains (Fig. ~~10~~11). This would imply that the emplacement of the high-density bodies also predates the propagation of the MMF. Such an interpretation would support the previously proposed hypothesis that the NAFZ reached the eastern part of the present-day Marmara Sea (Izmit) around 4 Ma before present, when the area was a domain of distributed (trans)tensional deformation, and started to propagate beneath the present-day Sea of Marmara as the MMF about 2.5 Ma ago (Le Pichon et al., 2014; 2015).

Another implication from density modelling is that the compositional and therefore also rheological heterogeneity of the Marmara crust may result in a differential response of the area to present-day far-field stresses. Accordingly, conclusions drawn from earlier studies investigating the stress-strain state in the region of the Marmara Sea (Hergert and Heidbach, 2010, 2011; Hergert et al., 2011) need to be ~~checked if there are still valid.~~revisited.

One of the important discussions in the area of the Marmara region is on aspects that govern the dynamics of the MMF, where a 250-year lasting seismic gap in the southern vicinity of Istanbul is observed. The western segment of the MMF is considered as a partially creeping segment (Schmittbuhl et al., 2016; Bohnhoff et al., 2017b), whereas the eastern-central segment of the MMF is thought to be locked down to 10 km depth (Bohnhoff et al., 2013; 2017b; Ergintav et al., 2014; Sakic et al., 2016). The reasons why this seismic gap of the MMF has not ruptured over the past 250 years are debated. The felsic to intermediate crustal composition deduced from our gravity model would favour creep between the two crustal high-density bodies, whereas the two domains of the high-density bodies could represent locked segments that would require high-stress levels to fail. In

case of failure, however, the energy would probably be released in a strong earthquake. These high-density bodies are interpreted as mafic and therefore represent stronger material than the surrounding felsic to intermediate crustal material of the same depth. Such rheological heterogeneities would explain the distribution of different deformation modes with creeping segments in the felsic to intermediate crustal domains and locked to critically stressed segments in the mafic domains. This hypothesis could have implications for hazard and risk assessment in this area, but need to be tested by geodynamic models considering thermo-mechanical principles.

## 6. Conclusions

In this study, ~~a~~ 3D crustal density ~~model~~ configurations are presented for the Sea of Marmara ~~was presented~~ that ~~integrates~~integrate available seismological observations and ~~is~~are consistent with observed gravity. Testing successively models of increasing complexity, ~~a~~three best-fit ~~model is~~models are derived that ~~resolves~~resolve six ~~structural~~crustal units with different densities (Table 1). From our results we conclude:

(1) The present-day seafloor of the Marmara Sea has a more complex structure than during the phase of its initiation and is structured into the three main depocentres of the Tekirdağ Basin, the Central Basin, and the Çınarcık Basin. ~~This structural pattern is consistent with a pull-apart setting in a releasing zone of the NAFZ.~~

(2) Below the present-day seafloor, the unit of syn-kinematic sediments of the Marmara Sea indicates that two main depocentres were subsiding during the early phase of basin formation. A lower sedimentary unit is interpreted as pre-kinematic sediments of the Marmara Sea. The sedimentary units are underlain by ~~the~~a felsic ~~metamorphic~~ upper crystalline crust that is significantly thinned below the basin. The lowest crustal layer of regional extent is the intermediate to mafic lower crystalline crust. Both crystalline crustal layers are cut by two up-doming high-density ~~mafic~~ bodies that rise from the Moho to ~~the base of the syn-kinematic basins. The Moho surface used in this study is consistent with the satellite gravity observation.~~ relatively shallow depths.

(3) The emplacement of the high-density bodies within the crystalline crust could have a causal relationship with the basin-forming mechanism.

(4) The spatial correlation between the high-density bodies with the bent segments along the MMF indicates that rheological contrasts in the crust may control the propagation and movement of the MMF; these high-density bodies are a possible explanation for the bends of the MMF, and support the hypothesis that the MMF is geomechanically segmented.

(5) The high-density bodies may have an impact on the stress variability along the MMF. Therefore, ~~an update of the existing~~ geomechanical ~~model is now essential to~~ models of the area should account for ~~this more detailed~~lateral variations in crustal density ~~distribution. In addition,~~.

*Competing interests.* The authors declare that they have no conflict of interest.

*Acknowledgements.* The research leading to these results was conducted under the ~~3D density model could be considered for further thermo-mechanical modelling~~auspices of the ~~system dynamics.~~*ALErT initiative (Anatolian pLateau climatE and Tectonic hazards)*, an Initial Training Network (ITN) financed by the People Programme (Marie Curie Actions) of the European Union's Seventh Framework Programme FP7/2007- 2013/ under REA grant agreement no. 607996. We are indebted to Pierre Henry for his supportive comments as a referee and his contribution of the "Improved–TOPEX" gravity dataset and the structural model of Kende at al. (2017) including the high resolution bathymetry grid. We are thankful to Mathieu Rodriguez and one anonymous referee for providing insightful reviews and constructive comments, which improved the quality of this manuscript. We also would like to acknowledge the comments of Hans-Jürgen Götze in the open discussion.

## References

Akbayram, K., Sorlien, C.C. and Okay, A.I.: Evidence for a minimum 52±1 km of total offset along the northern branch of the North Anatolian Fault in northwest Turkey. Tectonophysics, 668, 35–41, doi: 10.1016/j.tecto.2015.11.026, 2016.Akbayram, K., Şengör, A.C. and Özcan, E.: The evolution of the Intra-Pontide suture: implications of the discovery of late Cretaceous–early Tertiary melanges. Geological Society of America Special Papers, 525, SPE525–18, doi: 10.1130/2016.2525(18), 2016.

Aksoy, R.: Stratigraphy of the Marmara Island and Kapıdag Peninsula. Bulletin of Turkish Petroleum Geologists Society, (in Turkish), 7(1), 33–49, 1995.

Aksoy, R.: Mesoscopic tectonic features of the Marmara island and the Kapıdağı peninsula, NW Turkey. Turkish Journal of Earth Sciences, 5(3), 187–195, 1996.

Amante, C. and Eakins, B.W.: ETOPO1 1 Arc-Minute Global Relief Model: Procedures, Data Sources and Analysis, NOAA Technical Memorandum NESDIS NGDC-24, National Geophysical Data Center, NOAA, doi: 10.7289/V5C8276M, 2009.

Ambraseys, N.N.: Some characteristic features of the Anatolian fault zone, Tectonophysics, 9(2-3), 143–165, doi: 10.1016/0040-1951(70)90014-4, 1970.

Ambraseys, N.: The seismic activity of the Marmara Sea region over the last 2000 years, Bulletin of the Seismological Society of America, 92(1), 1–18, doi: 10.1785/0120000843, 2002.

Armijo, R., Meyer, B., Hubert, A. and Barka, A.: Westward propagation of the North Anatolian fault into the northern Aegean: Timing and kinematics, Geology, 27(3), 267–270, doi: 10.1130/0091-7613(1999)027<0267:WPOTNA>2.3.CO;2, 1999.

Armijo, R., Meyer, B., Navarro, S., King, G. and Barka, A.: Asymmetric slip partitioning in the Sea of Marmara pull-apart: A clue to propagation processes of the North Anatolian fault?, Terra Nova, 14(2), 80–86, doi: 10.1046/j.1365-3121.2002.00397.x, 2002.

Armijo, R., Pondard, N., Meyer, B., Uçarkus, G., de Lépinay, B.M., Malavieille, J., Dominguez, S., Gustcher, M.A., Schmidt, S., Beck, C. and Cagatay, N.: Submarine fault scarps in the Sea of Marmara pull-apart (North Anatolian Fault): Implications for seismic hazard in Istanbul, Geochemistry, Geophysics, Geosystems, 6(6), doi: 10.1029/2004GC000896, 2005.

Ates, A., Bilim, F., Buyuksarac, A., and Bektas, Ö.: A tectonic interpretation of the Marmara Sea, NW Turkey from geophysical data. Earth, Planets and Space, 60(3), 169–177, doi: 10.1186/BF03352780, 2008.

Ates, A., Kayiran, T. and Sincer, I.: Structural interpretation of the Marmara region, NW Turkey, from aeromagnetic, seismic and gravity data, Tectonophysics, 367, 41–99, doi: 10.1016/S0040-1951(03)00044-1, 2003.

Ates, A., Kearey, P., and Tufan, S.: New gravity and magnetic anomaly maps of Turkey. Geophysical Journal International, 136(2), 499–502, doi: 10.1046/j.1365-246X.1999.00732.x, 1999.

Attanasio, D., Brilli, M. and Bruno, M.: The properties and identification of marble from Proconnesos (Marmara Island, Turkey): a new database including isotopic, EPR and petrographic data, Archaeometry, 50(5), 747–774, doi: 10.1111/j.1475-4754.2007.00364.x, 2008.

Barka, A.: Slip distribution along the North Anatolian fault associated with the large earthquakes of the period 1939 to 1967, Bulletin of the Seismological Society of America, 86(5), 1238–1254, 1996.

Barka, A., Akyuz, H.S., Altunel, E., Sunal, G., Cakir, Z., Dikbas, A., Yerli, B., Armijo, R., Meyer, B., De Chabalier, J.B. and Rockwell, T.: The surface rupture and slip distribution of the 17 August 1999 Izmit earthquake (M 7.4), North Anatolian fault, Bulletin of the Seismological Society of America, 92(1), 43–60, doi: 10.1785/0120000841, 2002.

Barka, A.A. and Hancock, P.L.: Neotectonic deformation patterns in the convex-northwards arc of the North Anatolian faultzone, Geological Society, London, Special Publications, 17(1), 763–774, doi: 10.1144/GSL.SP.1984.017.01.61, 1984.

Barka, A.A. and Kadinsky-Cade, K.: Strike-slip fault geometry in Turkey and its influence on earthquake activity, Tectonics, 7(3), 663–684, doi: 10.1029/TC007i003p00663, 1988.

Barka, A. and Reilinger, R.: Active tectonics of the Eastern Mediterranean region: deduced from GPS, neotectonic and seismicity data, Annals of Geophysics, 40(3), doi: 10.4401/ag-3892, 1997.

Barthelmes, F. and Köhler, W.: International Centre for Global Earth Models (ICGEM), in: Drewes, H., Kuglitsch, F., Adám, J. et al., The Geodesists Handbook 2016, Journal of Geodesy (2016), 90(10), 907–1205, doi: 10.1007/s00190-016-0948-z, 2016.

Bayrakci, G.: Hétérogénéité 3D de la croûte supérieure sous la Mer de Marmara: tomographie sur une grille de sismomètres fond de mer et de profils de tirs (Doctoral dissertation, Paris, Institut de physique du globe), 2009.

Bayrakci, G., Laigle, M., Bécel, A., Hirn, A., Taymaz, T., Yolsal-Çevikbilen, S. and Team, S.: 3-D sediment-basement tomography of the Northern Marmara trough by a dense OBS network at the nodes of a grid of controlled source profiles along the North Anatolian fault, Geophysical Journal International, 194(3), 1335–1357, doi: 10.1093/gji/ggt211, 2013.

Bécel, A., Laigle, M., de Voogd, B., Hirn, A., Taymaz, T., Galvé, A., Shimamura, H., Murai, Y., Lépine, J.C., Sapin, M. and Özalaybey, S.: Moho, crustal architecture and deep deformation under the North Marmara Trough, from the SEISMARMARA Leg 1 offshore–onshore reflection–refraction survey, Tectonophysics, 467(1-4), 1–21, doi: 10.1016/j.tecto.2008.10.022, 2009.

Bécel, A., Laigle, M., De Voogd, B., Hirn, A., Taymaz, T., Yolsal-Cevikbilen, S. and Shimamura, H.: North Marmara Trough architecture of basin infill, basement and faults, from PSDM reflection and OBS refraction seismics, Tectonophysics, 490(1-2), 1–14, doi: 10.1016/j.tecto.2010.04.004, 2010.

Bohnhoff, M., Bulut, F., Dresen, G., Malin, P.E., Eken, T. and Aktar, M.: An earthquake gap south of Istanbul. Nature communications, 4, doi: 10.1038/ncomms2999, 2013.

Bohnhoff, M., Martínez-Garzón, P., Bulut, F., Stierle, E. and Ben-Zion, Y.: Maximum earthquake magnitudes along different sections of the North Anatolian fault zone, Tectonophysics, 674, 147–165, doi: 10.1016/j.tecto.2016.02.028, 2016a.

Bohnhoff, M., Ickrath, M. & Dresen, G.: Seismicity distribution in conjunction with spatiotemporal variations of coseismic slip and postseismic creep along the combined 1999 Izmit-Düzce rupture, Tectonophysics, doi: 10.1016/j.tecto.2016.07.029, 2016b.

Bohnhoff, M., Dresen, G., Ceken, U., Kadirioglu, F.T., Kartal, R.F., Kilic, T., Nurlu, M., Yanik, K., Acarel, D., Bulut, F. and Ito, H.: GONAF–the borehole Geophysical Observatory at the North Anatolian Fault in the eastern Sea of Marmara, Scientific Drilling, 22, 19–28, doi: 10.5194/sd-22-19-2017, 2017a.

Bohnhoff, M., Wollin, C., Domigall, D., Küperkoch, L., Martínez-Garzón, P., Kwiatek, G., Dresen, G. and Malin, P.E.: Repeating Marmara Sea earthquakes: indication for fault creep, Geophysical Journal International, 210(1), 332–339, doi: 10.1093/gji/ggx169, 2017b.

Brocher, T.M.: Empirical relations between elastic wavespeeds and density in the Earth's crust, Bulletin of the seismological Society of America, 95(6), 2081–2092, doi: 10.1785/0120050077, 2005.

Bürgmann, R., Ergintav, S., Segall, P., Hearn, E.H., McClusky, S., Reilinger, R.E., Woith, H. and Zschau, J.: Time-dependent distributed afterslip on and deep below the Izmit earthquake rupture, Bulletin of the Seismological Society of America, 92(1), 126–137, doi: 10.1785/0120000833, 2002.

Carton, H., Singh, S.C., Hirn, A., Bazin, S., De Voogd, B., Vigner, A., Ricolleau, A., Cetin, S., Oçakoğlu, N., Karakoç, F. and Sevilgen, V.: Seismic imaging of the three-dimensional architecture of the Çınarcık basin along the North Anatolian fault, Journal of Geophysical Research: Solid Earth, 112(B6), doi: 10.1029/2006JB004548, 2007.

Corsini, M. and Rolland, Y.: Late evolution of the southern European Variscan belt: exhumation of the lower crust in a context of oblique convergence, Comptes Rendus Geoscience, 341(2-3), 214–223, doi: 10.1016/j.crte.2008.12.002, 2009.

Christensen, N.I. and Mooney, W.D.: Seismic velocity structure and composition of the continental crust: A global view, Journal of Geophysical Research: Solid Earth, 100(B6), 9761–9788, doi: 10.1029/95JB00259, 1995.

Elmas, A.: Late Cenozoic tectonics and stratigraphy of northwestern Anatolia: the effects of the North Anatolian Fault to the region, International Journal of Earth Sciences, 92(3), 380–396, doi: 10.1007/s00531-003-0322-2, 2003.

Elmas, A. and Yiğitbaş, E.: Ophiolite emplacement by strike-slip tectonics between the Pontide Zone and the Sakarya Zone in northwestern Anatolia, Turkey, International Journal of Earth Sciences, 90(2), 257–269, doi: 10.1007/s005310000129, 2001.

Ergintav, S., Reilinger, R.E., Çakmak, R., Floyd, M., Cakir, Z., Doğan, U., King, R.W., McClusky, S. and Özener, H.: Istanbul's earthquake hot spots: Geodetic constraints on strain accumulation along faults in the Marmara seismic gap, Geophysical Research Letters, 41(16), 5783–5788, doi: 10.1002/2014GL060985, 2014.

Ergün, M. and Özel, E.: Structural relationship between the Sea of Marmara basin and the North Anatolian Fault Zone, Terra Nova, 7(2), 278–288, doi: 10.1111/j.1365-3121.1995.tb00695.x, 1995.

Faccenna, C., Bellier, O., Martinod, J., Piromallo, C. and Regard, V.: Slab detachment beneath eastern Anatolia: A possible cause for the formation of the North Anatolian fault. Earth and Planetary Science Letters, 242(1-2), 85–97, doi: 10.1016/j.epsl.2005.11.046, 2006.

Förste, C., Bruinsma, S., Abrikosov, O., Lemoine, J., Marty, J., Flechtner, F., Balmino, G., Barthelmes, F., and Biancale, R.: EIGEN-6C4 The latest combined global gravity field model including GOCE data up to degree and order 2190 of GFZ Potsdam and GRGS Toulouse, GFZ Data Services, doi: c10.5880/icgem.2015.1, 2014.

Genç, Ş.C.: Evolution of the Bayramiç magmatic complex, northwestern Anatolia, Journal of Volcanology and Geothermal Research, 85(1), 233–249, doi: 10.1016/S0377-0273(98)00057-2, 1998.

Hergert, T. and Heidbach, O.: Slip-rate variability and distributed deformation in the Marmara Sea fault system, Nature Geoscience, 3(2), 132, doi: 10.1038/ngeo739, 2010.

Hergert, T. and Heidbach, O.: Geomechanical model of the Marmara Sea region–II. 3-D contemporary background stress field, Geophysical Journal International, 185(3), 1090–1102, doi: 10.1111/j.1365-246X.2011.04992.x, 2011.

Hergert, T., Heidbach, O., Becel, A., and Laigle, M.: Geomechanical model of the Marmara Sea region–I. 3-D contemporary kinematics, Geophysical Journal International, 185(3), 1073–1089, doi: 10.1111/j.1365-246X.2011.04991.x, 2011.

Hirn, A. and Singh, S.: SEISMARMARA cruise, RV Le Nadir, doi: 10.17600/1080050, 2001.

Ince, E. S., Barthelmes, F., Reißland, S., Elger, K., Förste, C., Flechtner, F., and Schuh, H.: ICGEM – 15 years of successful collection and distribution of global gravitational models, associated services and future plans, Earth Syst. Sci. Data Discuss., doi: 10.5194/essd-2019-17, in review, 2019.

Janssen, C., Bohnhoff, M., Vapnik, Y., Görgün, E., Bulut, F., Plessen, B., Pohl, D., Aktar, M., Okay, A.I. and Dresen, G.: Tectonic evolution of the Ganos segment of the North Anatolian Fault (NW Turkey), Journal of Structural Geology, 31(1), 11–28, doi: 10.1016/j.jsg.2008.09.010, 2009.

Jolivet, L., Beyssac, O., Goff, B., Avigad, D., Lepvrier, C.: Oligo-Miocene midcrustal subhorizontal shear zone in indochina. Tectonics 20, 46, doi: 10.1029/2000TC900021, 2001.

Jolivet, L., Faccenna, C., Huet, B., Labrousse, L., Le Pourhiet, L., Lacombe, O., Lecomte, E., Burov, E., Denèle, Y., Brun, J.P. and Philippon, M.: Aegean tectonics: Strain localisation, slab tearing and trench retreat. Tectonophysics, 597, 1–33, doi: 10.1016/j.tecto.2012.06.011, 2013.

Karacık, Z., Yılmaz, Y., Pearce, J.A. and Ece, Ö.I.: Petrochemistry of the south Marmara granitoids, northwest Anatolia, Turkey, International Journal of Earth Sciences, 97(6), 1181–1200, doi: 10.1007/s00531-007-0222-y, 2008.

~~Kurtuluş, C.~~Kende, J., Henry, P., Bayrakci, G., Özeren, M. S., and Grall, C.: Moho depth and crustal thinning in the Marmara Sea region from gravity data inversion, J. Geophys. Res. Solid Earth, 122, 1381–1401, doi: 10.1002/2015JB012735, 2017.Kurtuluş, C. and Canbay, M.M.: Tracing the middle strand of the North Anatolian Fault Zone through the southern Sea of Marmara based on seismic reflection studies, Geo-Marine Letters, 27(1), 27–40, doi: 10.1007/s00367-006-0050-2, 2007.

Laigle, M., Bécel, A., de Voogd, B., Hirn, A., Taymaz, T. and Ozalaybey, S.: A first deep seismic survey in the Sea of Marmara: Deep basins and whole crust architecture and evolution, Earth and Planetary Science Letters, 270(3-4), 168–179, doi: 10.1016/j.epsl.2008.02.031, 2008.

Labrousse, L., Jolivet, L., Andersen, T.B., Agard, P., Hebert, R., Maluski, H., Schärer, U.: Pressure–temperature–time deformation history of the exhumation of ultra-high pressure rocks in the Western Gneiss Region, Norway. In: Whitney, D.L., Teyssier, C., Siddoway, C.S. (Eds.), Gneiss Domes in Orogeny. Spec. Pap. Geol. Soc. Am., 380, 155–182, doi: 10.1130/0-8137-2380-9.155, 2004.

Leloup, P.H., Lacassin, R., Tapponnier, P., Schärer, U., Zhong, D., Liu, X., Zhang, L., Ji, S., Trinh, P.T.: The Ailao Shan-Red River shear zone (Yunnan, China), Tertiary transform boundary of Indochina, Tectonophysics 251, 3–84, doi: 10.1016/0040-1951(95)00070-4, 1995.

Le Pichon, X., Chamot-Rooke, N., Rangin, C. and Şengör, A.C.: The North Anatolian fault in the sea of marmara, Journal of Geophysical Research: Solid Earth, 108(B4), doi: 10.1029/2002JB001862, 2003.

Le Pichon, X., Imren, C., Rangin, C., Şengör, A.C. and Siyako, M.: The South Marmara Fault, International Journal of Earth Sciences, 103(1), 219–231, doi: 10.1007/s00531-013-0950-0, 2014.

Le Pichon, X., Şengör, A.C., Demirbağ, E., Rangin, C., Imren, C., Armijo, R., Görür, N., Çağatay, N., De Lepinay, B.M., Meyer, B. and Saatçılar, R.: The active main Marmara fault, Earth and Planetary Science Letters, 192(4), 595–616, doi: 10.1016/S0012-821X(01)00449-6, 2001.

Le Pichon, X., Şengör, A.C., Kende, J., İmren, C., Henry, P., Grall, C. and Karabulut, H.: Propagation of a strike-slip plate boundary within an extensional environment: the westward propagation of the North Anatolian Fault, Canadian Journal of Earth Sciences, 53(11), 1416–1439, doi: 10.1139/cjes-2015-0129, 2015.

Le Pourhiet, L., Huet, B., May, D.A., Labrousse, L. and Jolivet, L.: Kinematic interpretation of the 3d shapes of metamorphic core complexes. Geochemistry, Geophysics, Geosystems, 13(9), doi: 10.1029/2012GC004271, 2012.

Le Pourhiet, L., Huet, B. and Traore, N.: Links between long-term and short-term rheology of the lithosphere: Insights from strike-slip fault modelling, Tectonophysics, 631, 146–159, doi: 10.1016/j.tecto.2014.06.034, 2014.

Ludwig, W. J., Nafe, J. E., and Drake C. L.: Seismic refraction, in The Sea, A. E. Maxwell (Editor), Vol. 4, Wiley-Interscience, New York, 53–84, 1970.

Maystrenko, Y.P. and Scheck-Wenderoth, M.: 3D lithosphere-scale density model of the Central European Basin System and adjacent areas, Tectonophysics, 601, 53–77, doi: 10.1016/j.tecto.2013.04.023, 2013.

Maystrenko, Y.P., Scheck-Wenderoth, M., Hartwig, A., Anka, Z., Watts, A.B., Hirsch, K.K. and Fishwick, S.: Structural features of the Southwest African continental margin according to results of lithosphere-scale 3D gravity and thermal modelling, Tectonophysics, 604, 104–121, doi: 10.1016/j.tecto.2013.04.014, 2013.

McKenzie, D.: Active tectonics of the Mediterranean region, Geophysical Journal of the Royal Astronomical Society, 30(2), 109–185, doi: 10.1111/j.1365-246X.1972.tb02351.x, 1972.

MediMap Group: Morpho-bathymetry of the Mediterranean Sea, special publication, Atlases and Maps, two maps at 1/2000000, CIESM/Ifremer, Issy-les-Moulineaux, France, 2005.

Murru, M., Akinci, A., Falcone, G., Pucci, S., Console, R. and Parsons, T.: M≥ 7 earthquake rupture forecast and time-dependent probability for the Sea of Marmara region, Turkey, Journal of Geophysical Research: Solid Earth, 121(4), 2679–2707, doi: 10.1002/2015JB012595, 2016.

Okay, A.I. and Tüysüz, O.; Tethyan sutures of northern Turkey. Geological Society, London, Special Publications, 156(1), 475–515, doi: 10.1144/GSL.SP.1999.156.01.221, 1999.

Parke, J.R., White, R.S., McKenzie, D., Minshull, T.A., Bull, J.M., Kuşçu, İ., Görür, N. and Şengör, C.: Interaction between faulting and sedimentation in the Sea of Marmara, western Turkey, Journal of Geophysical Research: Solid Earth, 107(B11), EPM-2, doi: 10.1029/2001JB000450, 2002.

Parsons, T.: Recalculated probability of M ≥ 7 earthquakes beneath the Sea of Marmara, Turkey, Journal of Geophysical Research: Solid Earth, 109(B5), doi: 10.1029/2003JB002667, 2004.

Pavlis, N. K.,Holmes, S. A., Kenyon, S. C. and Factor, J. K. : The development and evaluation of the earth gravitational model 2008 (EGM2008), Journal of Geophysical Research: Solid Earth, 117(B4), doi: 10.1029/2011JB008916, 2012.

Pucci, S., Palyvos, N., Zabci, C., Pantosti, D. and Barchi, M.: Coseismic ruptures and tectonic landforms along the Düzce segment of the North Anatolian Fault Zone (Ms 7.1, November 1999), Journal of Geophysical Research: Solid Earth, 111(B6), doi: 10.1029/2004JB003578, 2006.

Robertson, A.H. and Ustaömer, T.: Tectonic evolution of the Intra-Pontide suture zone in the Armutlu Peninsula, NW Turkey. Tectonophysics, 381(1-4), 175–209, doi: 10.1016/j.tecto.2002.06.002, 2004.

Reilinger, R.E., McClusky, S.C., Oral, M.B., King, R.W., Toksoz, M.N., Barka, A.A., Kinik, I., Lenk, O. and Sanli, I.: Global Positioning System measurements of present-day crustal movements in the Arabia-Africa-Eurasia plate collision zone, Journal of Geophysical Research: Solid Earth, 102(B5), 9983–9999, doi: 10.1029/96JB03736, 1997.

Reilinger, R., McClusky, S., Vernant, P., Lawrence, S., Ergintav, S., Cakmak, R., Ozener, H., Kadirov, F., Guliuv, I., Stepanyan, R., Nadariya, M., Hahubia, G., Mahmoud, S., Sakr, K., ArRajehi, A., Paradissis, D., Al-Aydrus, A., Prilepin, M., Guseva, T., Evren, E., Dmitrotsa, A., Filikov, S.V., Gomez, F., Al-Ghazzi, R. and Karam, G.: GPS constraints on continental deformation in the Africa-Arabia-Eurasia continental collision zone and implications for the dynamics of plate interactions, Journal of Geophysical Research: Solid Earth, 111(B5), doi: 10.1029/2005JB004051, 2006.

Sakic, P., Piete, H., Ballu, V., Royer, J.Y., Kopp, H., Lange, D., Petersen, F., Özeren, M.S., Ergintav, S., Geli, L. and Henry, P.: No significant steady state surface creep along the North Anatolian Fault offshore Istanbul: Results of 6 months of seafloor acoustic ranging. Geophysical Research Letters, 43(13), 6817–6825, doi: 10.1002/2016GL069600, 2016.

Sandwell, D., Garcia, E., Soofi, K., Wessel, P., Chandler, M. and Smith, W.H.: Toward 1-mGal accuracy in global marine gravity from CryoSat-2, Envisat, and Jason-1. The Leading Edge, 32(8), 892–899, doi: 10.1190/tle32080892.1, 2013.

Sandwell, D.T., Müller, R.D., Smith, W.H., Garcia, E. and Francis, R.: New global marine gravity model from CryoSat-2 and Jason-1 reveals buried tectonic structure, Science, 346(6205), 65–67, doi: 10.1126/science.1258213, 2014.

Schmidt, S., Plonka, C., Götze, H.J. and Lahmeyer, B.: Hybrid modelling of gravity, gravity gradients and magnetic fields, Geophysical Prospecting, 59(6), 1046–1051, doi: 10.1111/j.1365-2478.2011.00999.x, 2011.

Schmittbuhl, J., Karabulut, H., Lengliné, O. and Bouchon, M.: Long-lasting seismic repeaters in the Central Basin of the Main Marmara Fault, Geophysical Research Letters, 43(18), 9527–9534, doi: 10.1002/2016GL070505, 2016.

~~Sippel, J., Scheck-Wenderoth, M., Lewerenz, B. and Kroeger, K.F.: A crust-scale 3D structural model of the Beaufort-Mackenzie Basin (Arctic Canada), Tectonophysics, 591, 30–51, doi: 10.1016/j.tecto.2012.10.030, 2013.~~

Şengör, A.C., Tüysüz, O., Imren, C., Sakınç, M., Eyidoğan, H., Görür, N., Le Pichon, X. and Rangin, C.: The North Anatolian fault: A new look. Annu. Rev. Earth Planet. Sci., 33, 37–112, doi: 10.1146/annurev.earth.32.101802.120415, 2005.

Sippel, J., Scheck-Wenderoth, M., Lewerenz, B. and Kroeger, K.F.: A crust-scale 3D structural model of the Beaufort-Mackenzie Basin (Arctic Canada), Tectonophysics, 591, 30–51, doi: 10.1016/j.tecto.2012.10.030, 2013.

Sobolev, S., Petrunin, A., Garfunkel, Z. and Babeyko, A.Y.: Thermo-mechanical model of the dead sea transform. Earth Planet. Sci. Lett. 238, 78–95, doi: 10.1016/j.epsl.2005.06.058, 2005.

Stein, R.S., Barka, A.A. and Dieterich, J.H.: Progressive failure on the North Anatolian fault since 1939 by earthquake stress triggering, Geophysical Journal International, 128(3), 594–604, doi: 10.1111/j.1365-246X.1997.tb05321.x, 1997.

Turgut, S. and Eseller, G.: Sequence stratigraphy, tectonics and depositional history in eastern Thrace Basin, NW Turkey, Marine and Petroleum Geology, 17(1), 61–100, doi: 10.1016/S0264-8172(99)00015-X, 2000.

Ustaömer, P.A., Ustaömer, T., Collins, A.S. and Reischpeitsch, J.: Lutetian arc-type magmatism along the southern Eurasian margin: new U-Pb LA-ICPMS and whole-rock geochemical data from Marmara Island, NW Turkey, Mineralogy and Petrology, 96(3-4), 177–196, doi: 10.1007/s00710-009-0051-8, 2009.

Ünay, E., Emre, Ö., Erkal, T. and Keçer, M.: The rodent fauna from the Adapazarı pull-apart basin (NW Anatolia): its bearings on the age of the North Anatolian Fault, Geodinamica Acta., 14(1-3), 169–75, doi: 10.1080/09853111.2001.11432442, 2001.

West, D.P. and Hubbard, M.S.: Progressive localization of deformation during exhumation of a major strike-slip shear zone: Norumbega fault zone, south-central Maine, USA, Tectonophysics 273, 185–201, doi: 10.1016/S0040-1951(96)00306-X, 1997.

Yaltırak, C.: Tectonic evolution of the Marmara Sea and its surroundings, Marine Geology, 190(1-2), 493–529, doi: 10.1016/S0025-3227(02)00360-2, 2002.

Yaltırak, C. and Alpar, B.: Evolution of the middle strand of North Anatolian Fault and shallow seismic investigation of the southeastern Marmara Sea (Gemlik Bay), Marine Geology, 190(1-2), 307–327, doi: 10.1016/S0025-3227(02)00352-3, 2002.

Yamamoto, Y., Takahashi, N., Pinar, A., Kalafat, D., Citak, S., Comoglu, M., Polat, R. and Kaneda, Y.: Geometry and segmentation of the North Anatolian Fault beneath the Marmara Sea, Turkey, deduced from long-term ocean bottom seismographic observations, Journal of Geophysical Research: Solid Earth, 122(3), 2069–2084, doi: 10.1002/2016JB013608, 2017.

Yildirim, C., Schildgen, T.F., Echtler, H., Melnick, D. and Strecker, M.R.: Late Neogene and active orogenic uplift in the Central Pontides associated with the North Anatolian Fault: Implications for the northern margin of the Central Anatolian Plateau, Turkey, Tectonics, 30(5), doi: 10.1029/2010TC002756, 2011.

Yildirim, C., Melnick, D., Ballato, P., Schildgen, T.F., Echtler, H., Erginal, A.E., Kıyak, N.G. and Strecker, M.R.: Differential uplift along the northern margin of the Central Anatolian Plateau: inferences from marine terraces, Quaternary Science Reviews, 81, 12–28, doi: 10.1016/j.quascirev.2013.09.011, 2013.

Yildirim, C. and Tüysüz, O.: Estimation of the long-term slip, surface uplift and block rotation along the northern strand of the North Anatolian Fault Zone: Inferences from geomorphology of the Almacık Block, Geomorphology, 297, 55–68, doi: 10.1016/j.geomorph.2017.08.038, 2017.

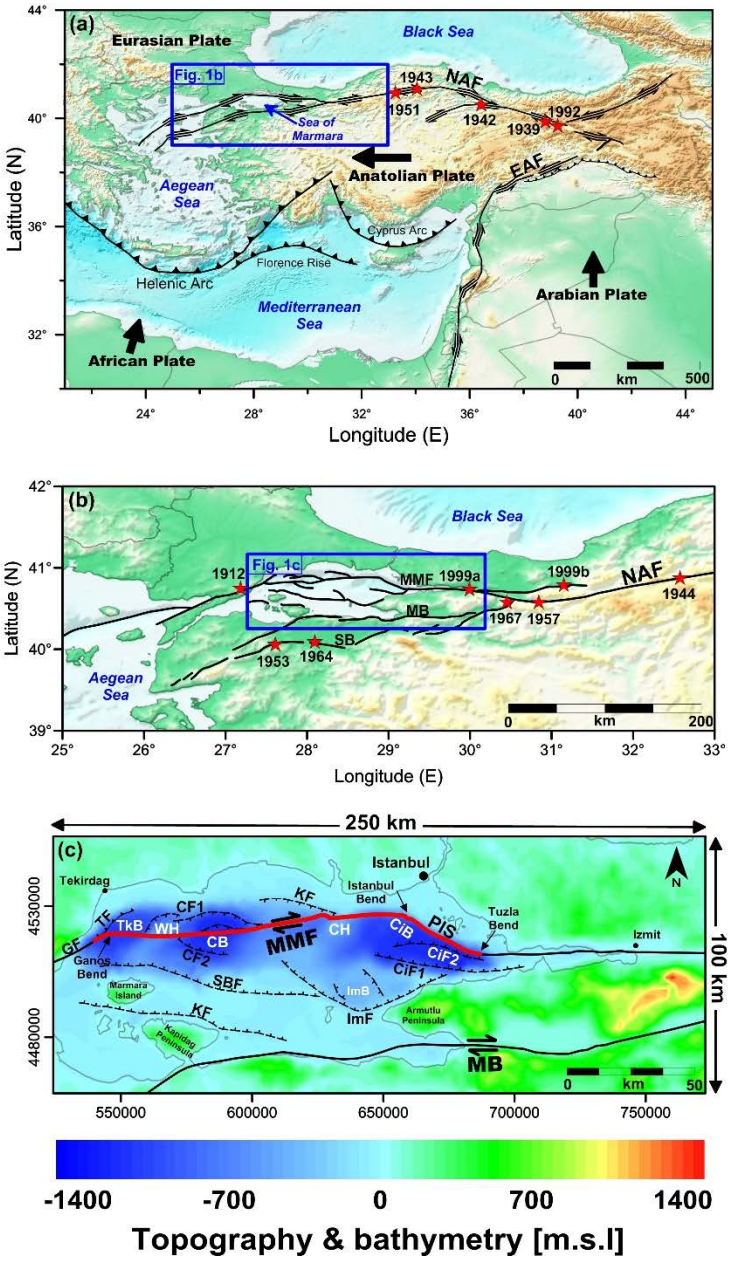
(a)
Eurasian Plate
Black Sea
Fig. 1b
1943
NAF
1951
1942
1992
1939
Sea of Marmara
Anatolian Plate
EAF
Aegean Sea
Cyprus Arc
Florence Rise
Helenic Arc
Arabian Plate
Mediterranean Sea
African Plate
0 km 500
Latitude (N)
Longitude (E)
(b)
Black Sea
Fig. 1c
1912
MMF
1999a
1999b
NAF
1944
MB
1967
1957
SB
1953
1964
Aegean Sea
0 km 200
Latitude (N)
Longitude (E)
250 km
(c)
Istanbul
Tekirdag
Istanbul Bend
Tuzla Bend
Izmit
N
TF
CF1
KF
TkB
WH
CB
MMF
CH
CiB
PiS
GF
CF2
CiF2
CiF1
Ganos Bend
Marmara Island
SBF
ImB
ImF
Armutlu Peninsula
Kapidag Peninsula
MB
0 km 50
100 km
4530000
4480000
550000
600000
650000
700000
750000
-1400
-700
0
700
1400
Topography & bathymetry [m.s.l]

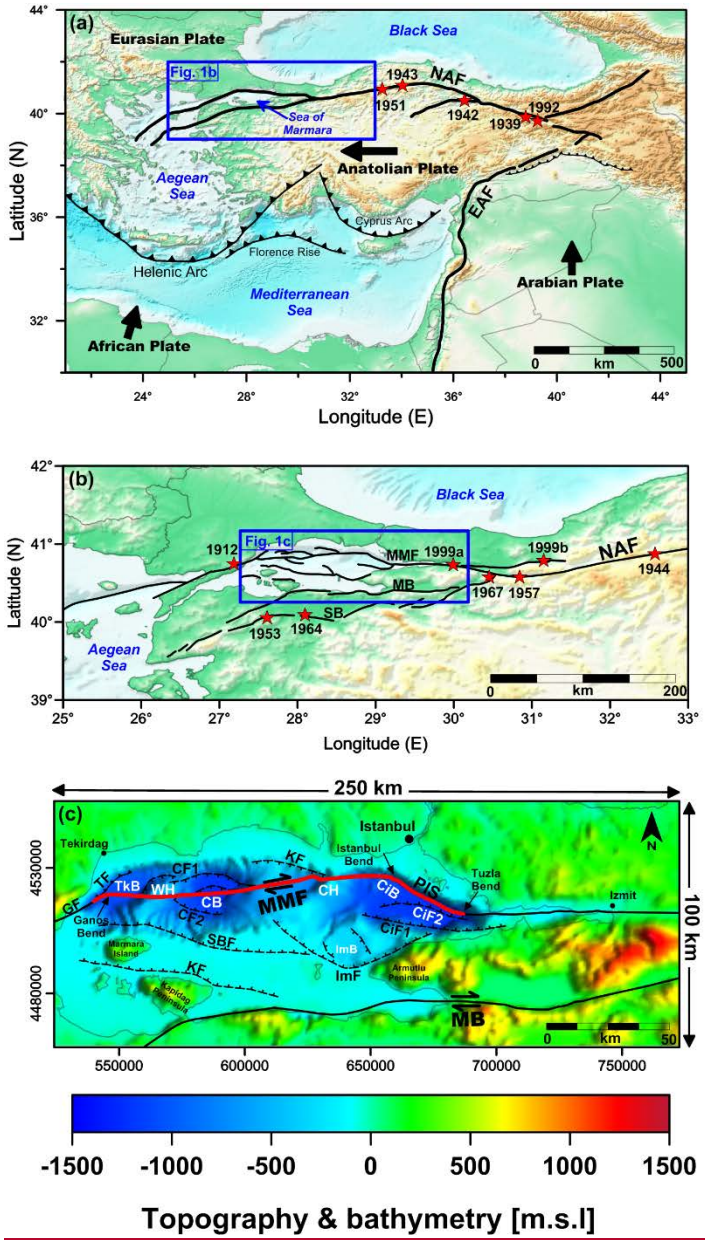


**Figure 1: ~~The location~~Location and ~~the~~ tectonic setting of the model area; (a) Plate ~~tectonics~~tectonic map of the Anatolian plate and its relation to the Arabian, African, and Eurasian Plates; (b) The NAFZ propagation and its branches in the NW Anatolian plate; (c) The model area (WGS84 UTM Zone 35N) including the relief map of the Sea of Marmara and its surrounding onshore domain, the seismic gap since 1766 (thick red line; Bohnhoff et. al., 2017b), and the faults system identified in the investigations by Armijo et al. (2002; 2005), and Carton et al. (2007). Topography and bathymetry from ETOPO1 (Amante and Eakins, 2009~~).~~) and Le Pichon et al. (2001). Abbreviations: North Anatolian Fault (NAF); Main Marmara Fault (MMF); Middle Branch of NAF (MB); Southern Branch (SB); Princes Islands Segment (PIS); Çınarcık Basin (CiB); Central Basin (CB); Tekirdağ Basin (TkB); Imralı Basin (ImB); Central High (CH); Western High (WH); Kapıdağ Fault (KF); Southern Border Fault (SBF); Imralı Fault (ImF); Çınarcık Faults**

**(CiF 1 & 2); Kumburgaz Fault (KF); Central Basin Faults (CF 1 & 2); Tekirdağ Fault (TF); Ganos Fault (GF). Red stars show the epicentres of major ~~events~~earthquakes (M > 6.5) during the past century.**

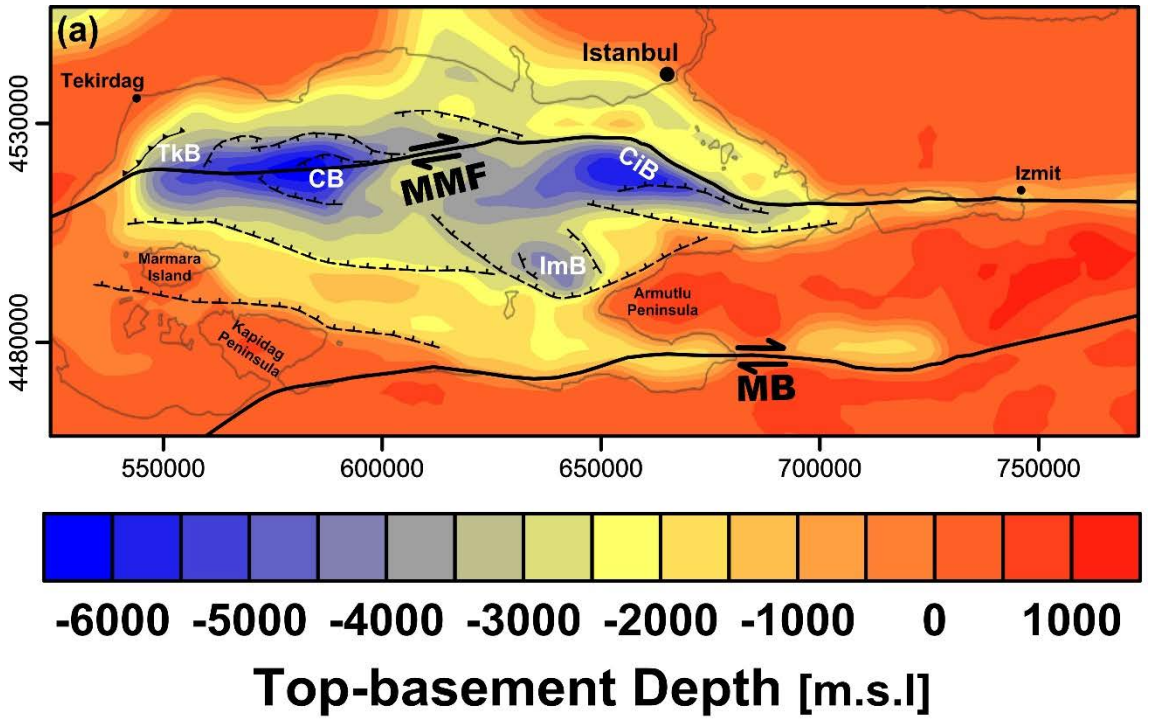
(a)
Istanbul
Tekirdag
TkB
CB
MMF
CiB
Izmit
ImB
Marmara Island
Armutlu Peninsula
Kapidag Peninsula
MB
4530000
4480000
550000
600000
650000
700000
750000
-6000 -5000 -4000 -3000 -2000 -1000 0 1000
Top-basement Depth [m.s.l]

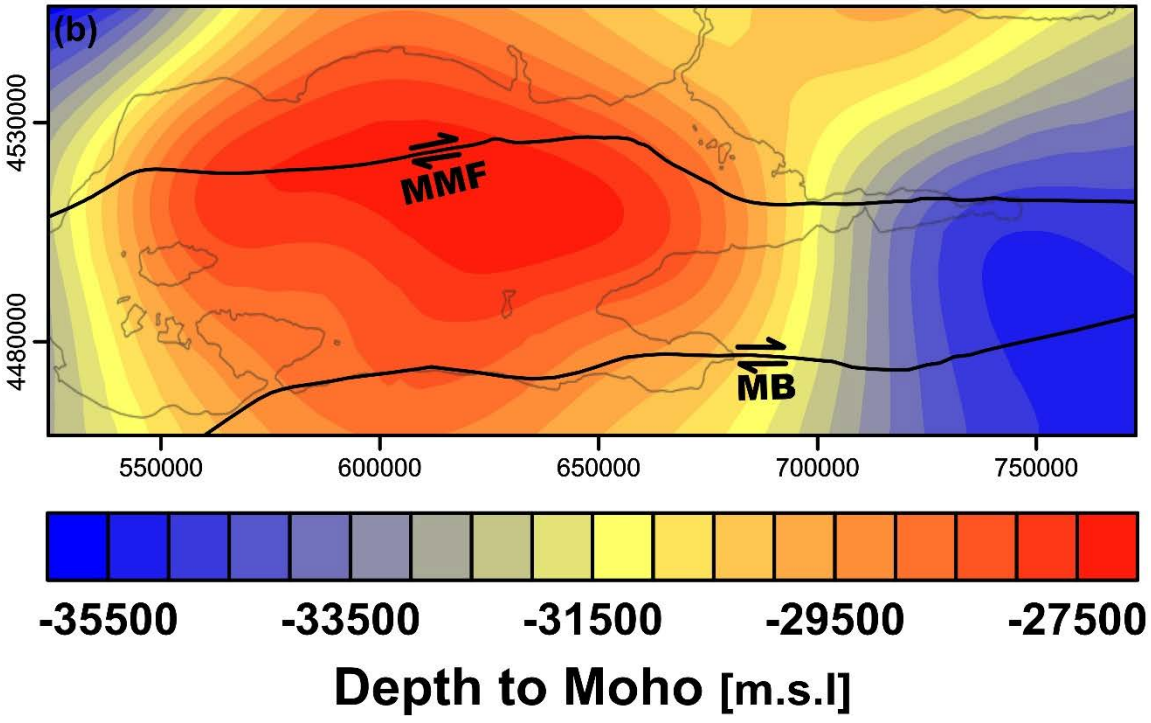
(b)
MMF
MB
4530000
4480000
550000
600000
650000
700000
750000
-35500 -33500 -31500 -29500 -27500
Depth to Moho [m.s.l]

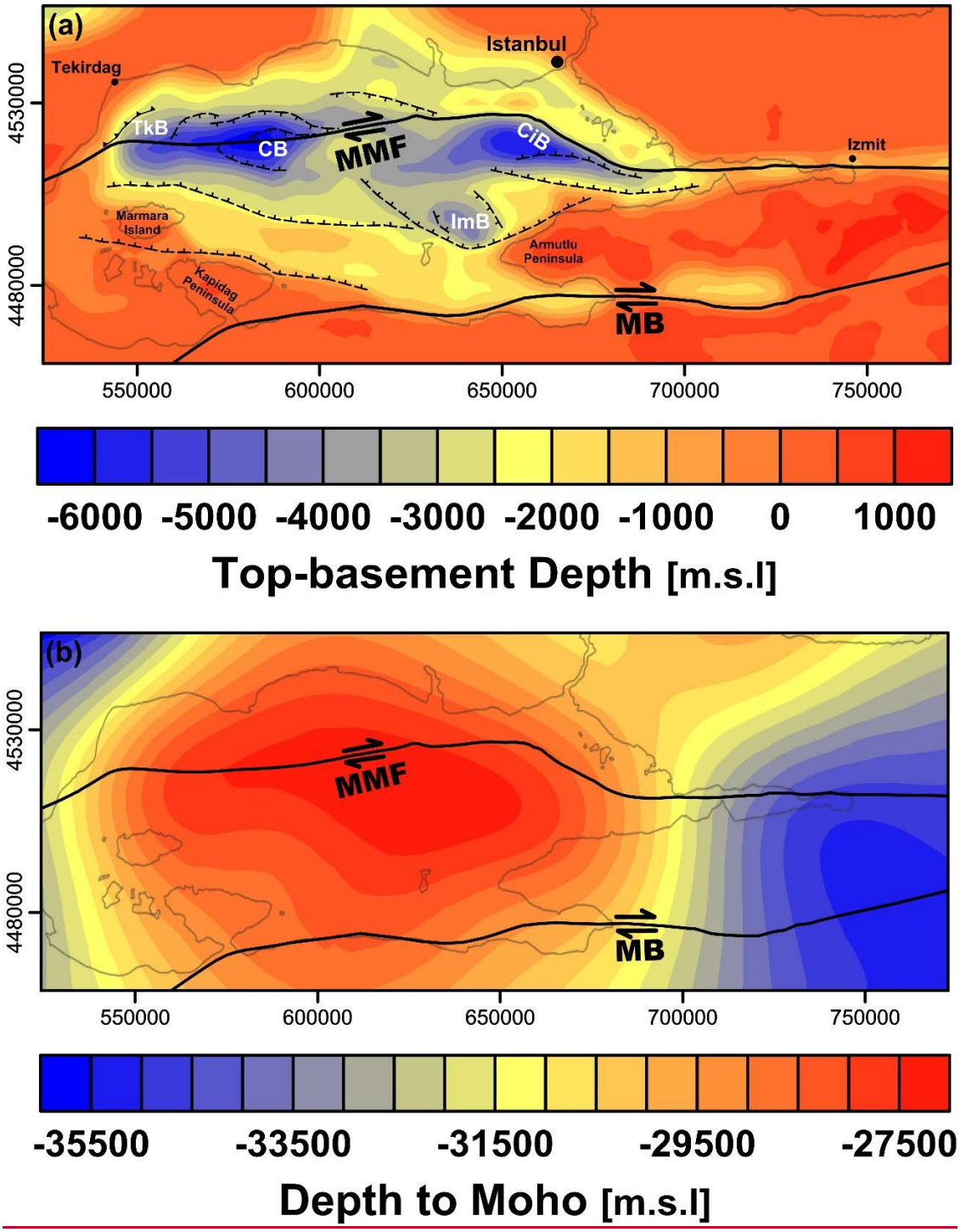


**Figure 2: Main horizons within the initial model (WGS84 UTM Zone 35N); (a) Depth to top-basement; (b) Depth to Moho. The corresponding thickness maps are illustrated in Fig. 3. Data from Hergert and Heidbach (2010). Abbreviations: Main Marmara Fault (MMF); Middle Branch of NAF (MB); Çınarcık Basin (CiB); Central Basin (CB); Tekirdağ Basin (TkB); Imralı Basin (ImB).**

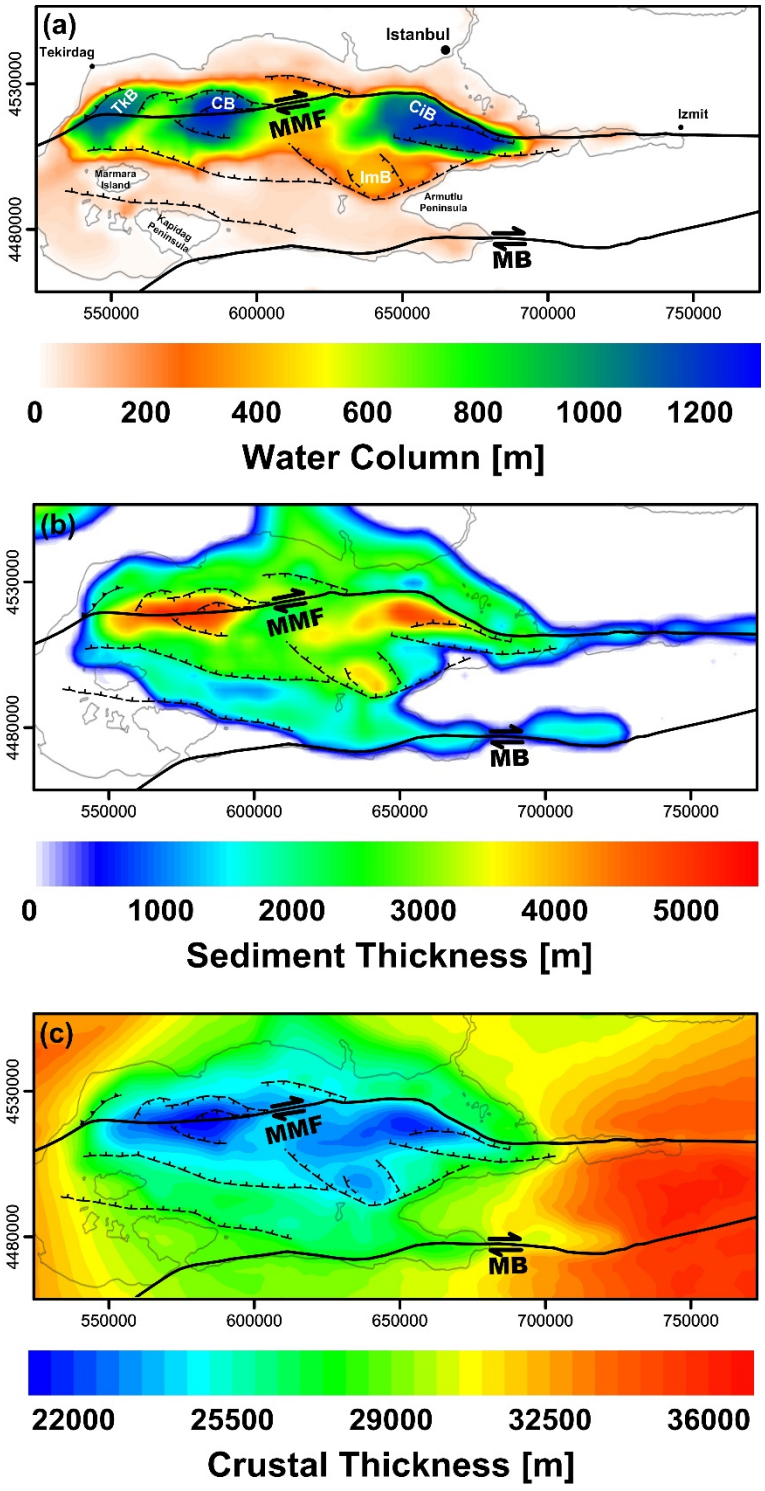
(a)
Istanbul
Tekirdag
Izmit
TkB
CB
MMF
CiB
ImB
Marmara Island
Armutlu Peninsula
Kapidag Peninsula
MB
4530000
4480000
550000
600000
650000
700000
750000
0
200
400
600
800
1000
1200
Water Column [m]
(b)
MMF
MB
0
1000
2000
3000
4000
5000
Sediment Thickness [m]
(c)
MMF
MB
22000
25500
29000
32500
36000
Crustal Thickness [m]

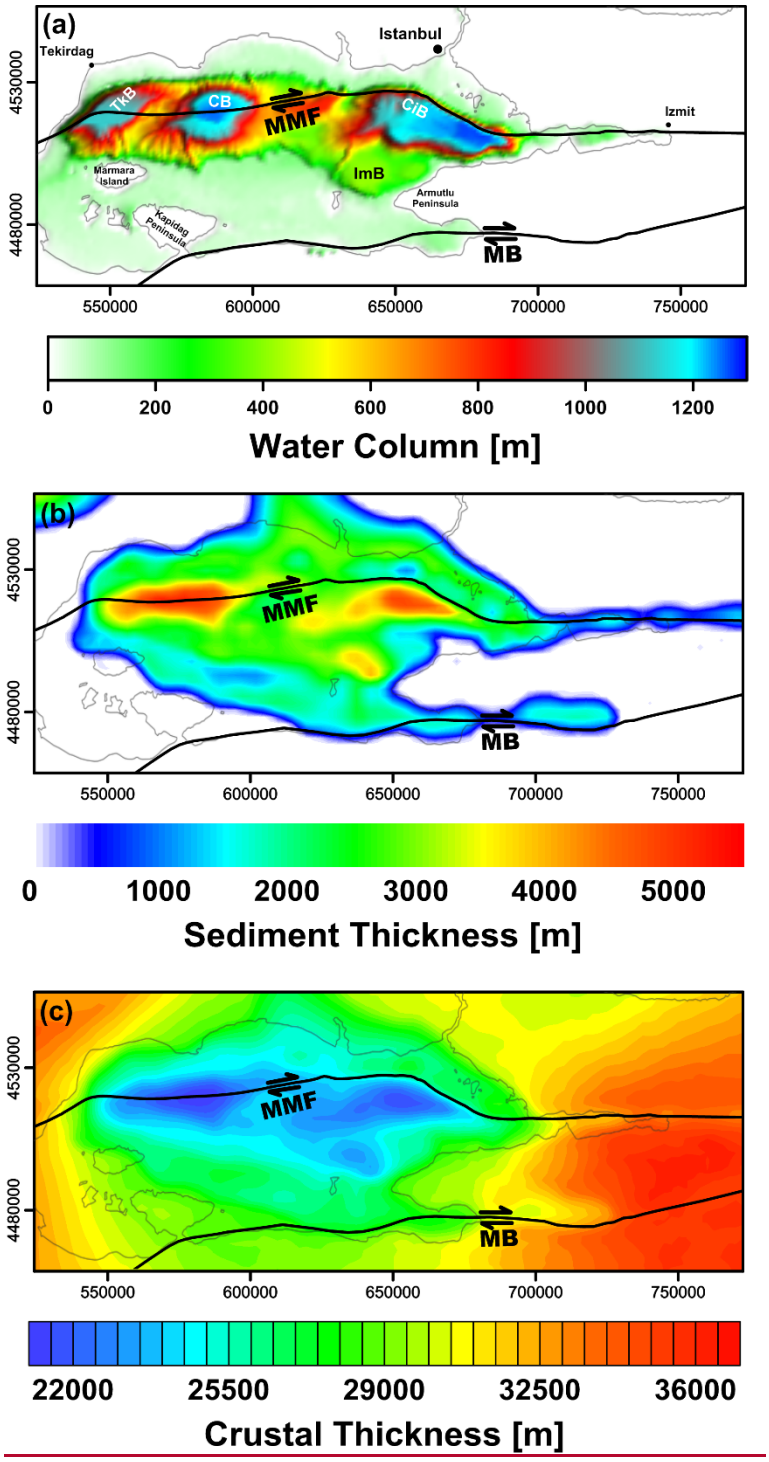
(a)
Istanbul
Tekirdag
Izmit
TkB
CB
MMF
CiB
ImB
Marmara Island
Armutlu Peninsula
Kapidag Peninsula
MB
4530000
4480000
550000
600000
650000
700000
750000
0
200
400
600
800
1000
1200
Water Column [m]
(b)
MMF
MB
0
1000
2000
3000
4000
5000
Sediment Thickness [m]
(c)
MMF
MB
22000
25500
29000
32500
36000
Crustal Thickness [m]

**Figure 3: Thickness distribution map of the initial structural model (WGS84 UTM Zone 35N): (a) Seawater column; (b) Syn-kinematic sediment thickness; (c) Homogeneous crustal thickness. Abbreviations: Main Marmara Fault (MMF); Middle Branch of NAF (MB); Çınarcık Basin (CiB); Central Basin (CB); Tekirdağ Basin (TkB); Imralı Basin (ImB).**

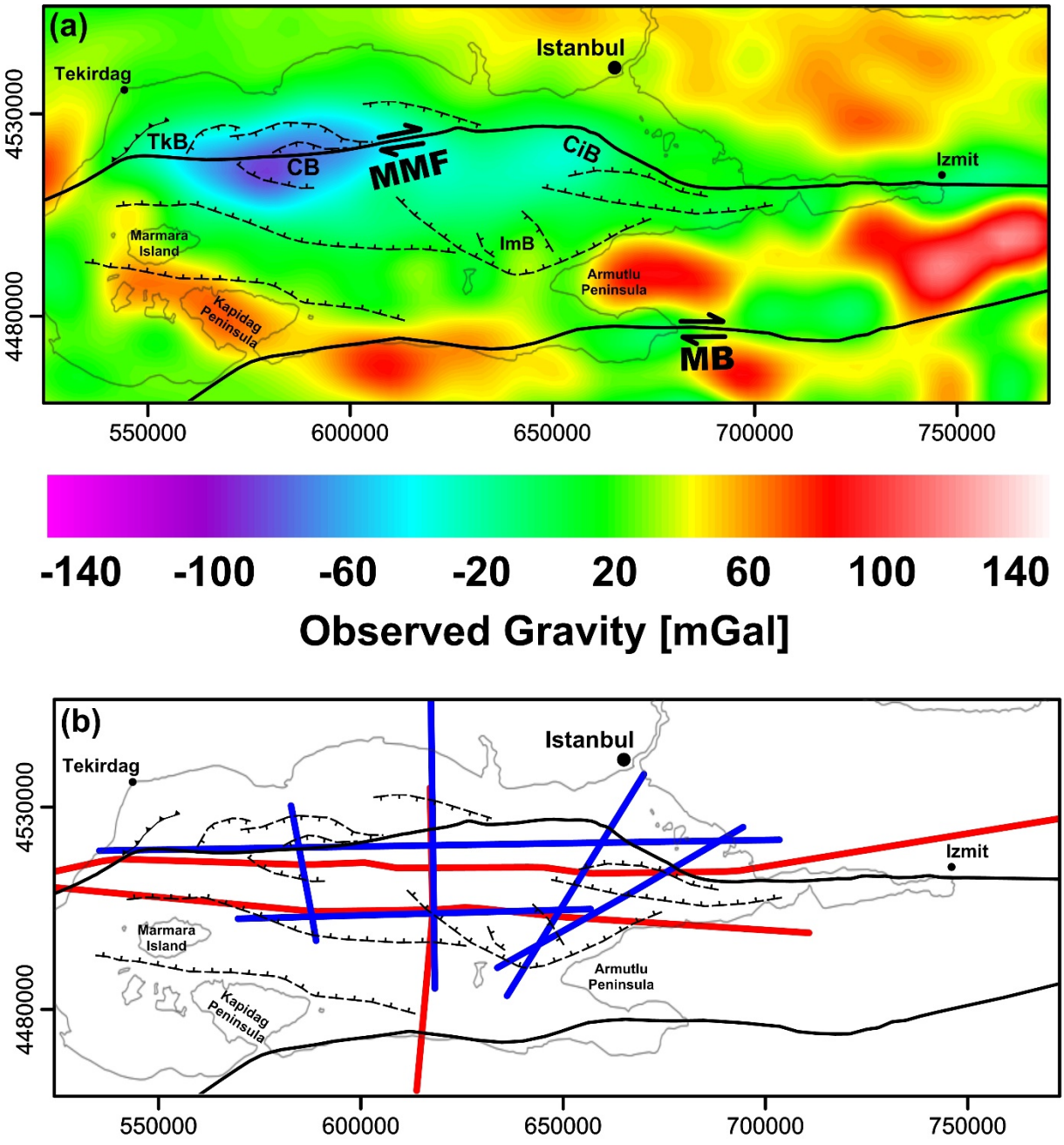
(a)
Istanbul
Tekirdag
TkB
CB
MMF
CiB
Izmit
ImB
Marmara Island
Armutlu Peninsula
Kapidag Peninsula
MB
4530000
4480000
550000
600000
650000
700000
750000
-140
-100
-60
-20
20
60
100
140
Observed Gravity [mGal]
(b)
Istanbul
Tekirdag
Izmit
Marmara Island
Armutlu Peninsula
Kapidag Peninsula
4530000
4480000
550000
600000
650000
700000
750000

~~Figure 4: Considered geophysical~~

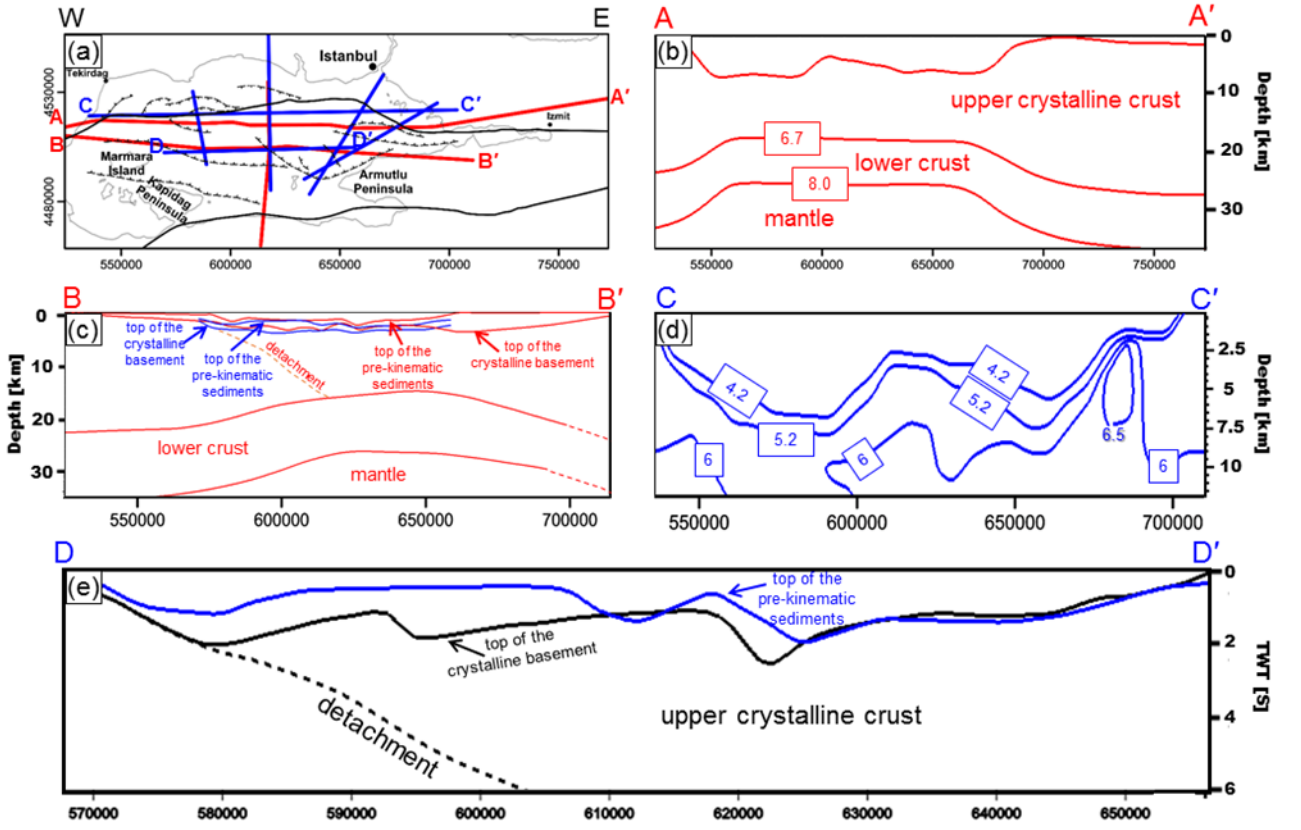


**Figure 4: Location of seismic profiles considered in this study and corresponding P-wave velocities and interpretations (modified after Laigle et al., 2008; Bécel et al., 2009; Bayrakci et al., 2013): (a) Location of the seismic profiles. Red lines are from reflection–refraction survey (Bécel et al., 2009) and blue lines are from sediment-basement tomography (Bayrakci et al., 2013); (b) Crustal structure and depth to Moho along the AA′ cross-section; (c) Crustal structure and depth to Moho along the BB′ cross-section including interpretations of the tomographic results along the DD′ profile; (d) P-wave velocity contours form the tomographic modelling along the CC′ profile; (d) Tomographic modelled isovelocity of 4.2 km.s$^{-1}$ (blue line) representing top of the pre-kinematic sediments in two way travel time along the DD′ profile and multichannel reflection seismic interpretation form Laigle et al. (2008) on the same profile. Numbers are modelled P-wave velocities for base syn-kinematic sediments (4.2 km.s$^{-1}$), base pre-kinematic-sediments (5.2 km.s$^{-1}$), top of the lower crust (6.7 km.s$^{-1}$), and the Moho discontinuity (8 km.s$^{-1}$).**

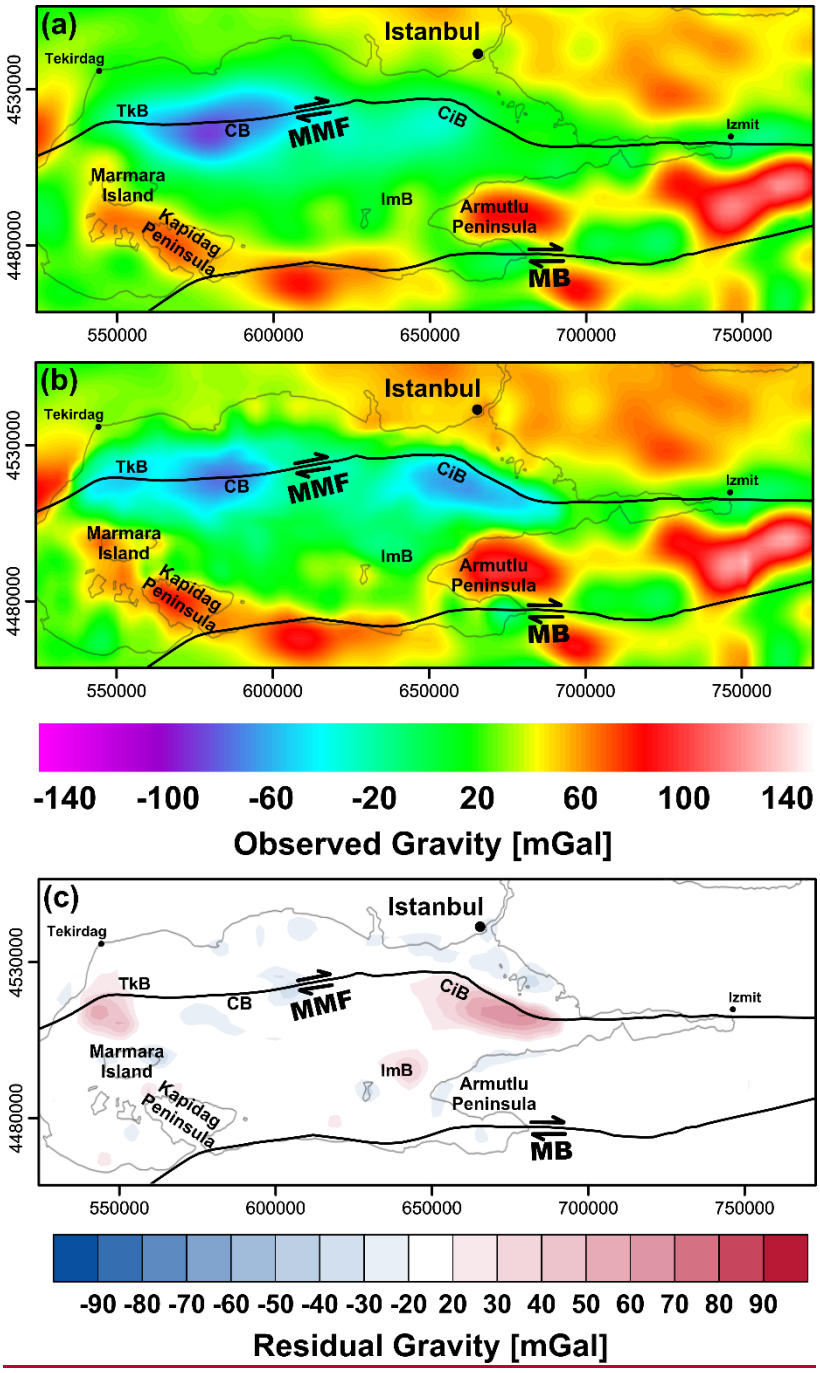


**Figure 5: Considered gravity datasets in this study (WGS84 UTM Zone 35N); (a) Observed satellite free-air anomaly (Eigen-6C4; Förste et al., ~~2014); (b) Seismic profiles across the model area. Red profiles are from wide-angle refraction-reflection survey (Bécel at al., 2009) and blue profiles are from 3D basement tomography inversion (Bayrakci et al., 2013).~~**

**2014); (b) Free-air anomaly map of "Improved–TOPEX" from Kende et al. (2017) combining the Jason-1 and CryoSat-2 satellite data (Sandwell et al., 2014) and the Marsite cruise gravity measurements over the Sea of Marmara. Onshore gravity of this dataset is based on EGM 2008 (Pavlis et al., 2012); (c) The difference between the two gravity datasets (a - b). Abbreviations: Main Marmara Fault (MMF); Middle Branch of NAF (MB); Çınarcık Basin (CiB); Central Basin (CB); Tekirdağ Basin (TkB); Imralı Basin (ImB).**

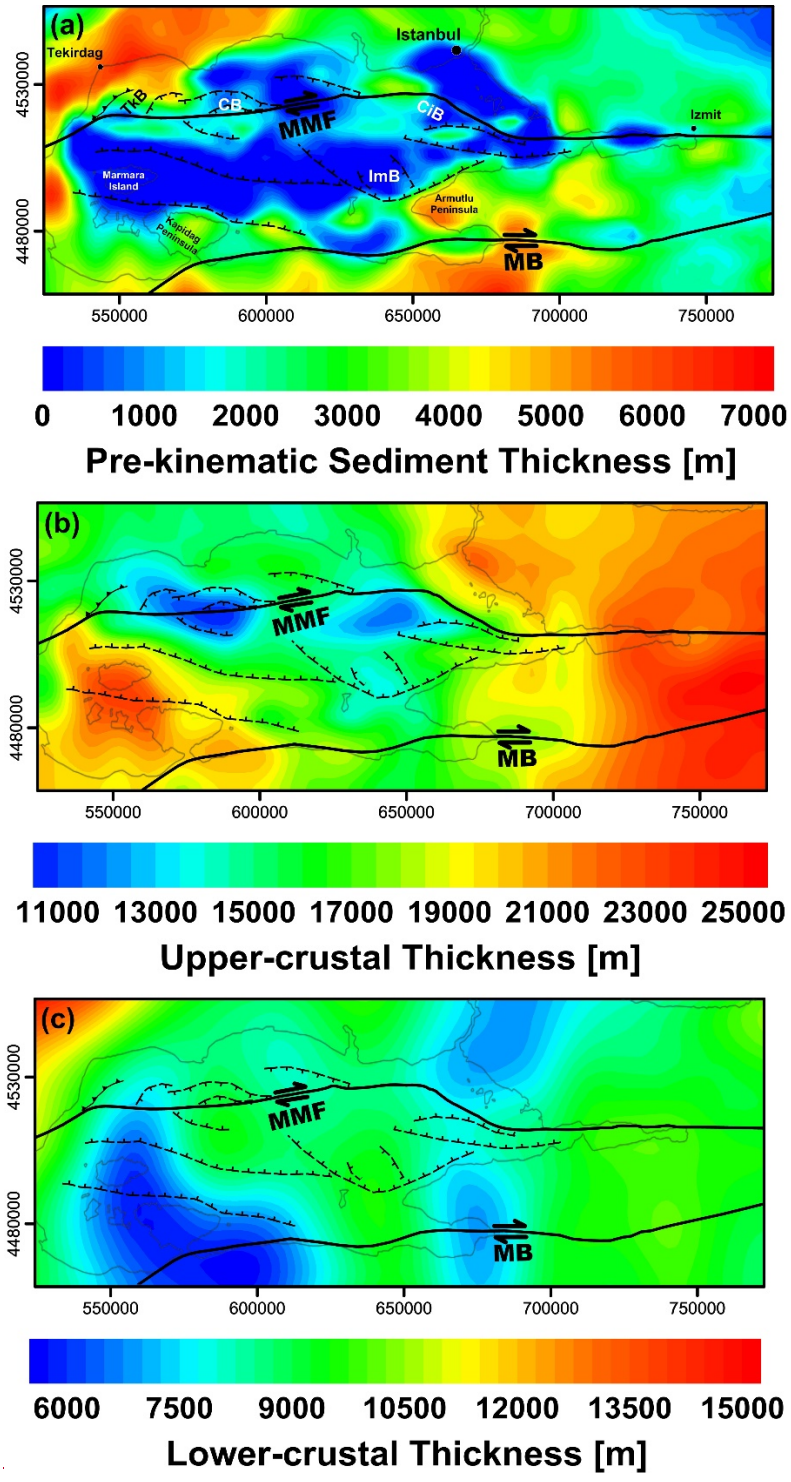
(a)
Tekirdag
Istanbul
Izmit
TkB
CB
MMF
CiB
ImB
Marmara Island
Armutlu Peninsula
Kapidag Peninsula
MB
4530000
4480000
550000
600000
650000
700000
750000
0 1000 2000 3000 4000 5000 6000 7000
Pre-kinematic Sediment Thickness [m]
(b)
MMF
MB
4530000
4480000
550000
600000
650000
700000
750000
11000 13000 15000 17000 19000 21000 23000 25000
Upper-crustal Thickness [m]
(c)
MMF
MB
4530000
4480000
550000
600000
650000
700000
750000
6000 7500 9000 10500 12000 13500 15000
Lower-crustal Thickness [m]

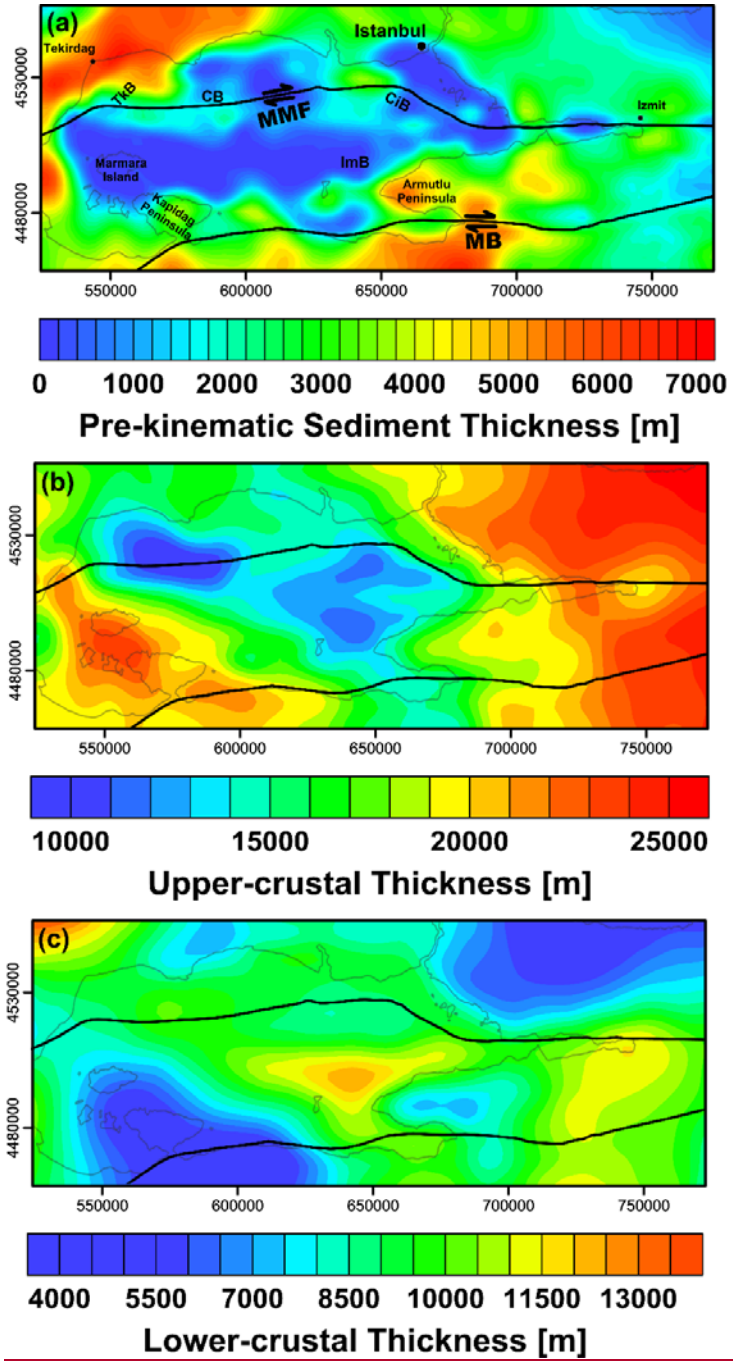


**Figure ~~5: Crustal~~6: Differentiated crustal structural model integrating seismic observations along the profiles in Fig. 4 (WGS84 UTM Zone 35N): (a) Pre-kinematic sediment thickness; (b) Upper crystalline crustal thickness; (c) Lower crystalline crustal thickness. Abbreviations: Main Marmara Fault (MMF); Middle Branch of NAF (MB); Çınarcık Basin (CiB); Central Basin (CB); Tekirdağ Basin (TkB); Imralı Basin (ImB).**

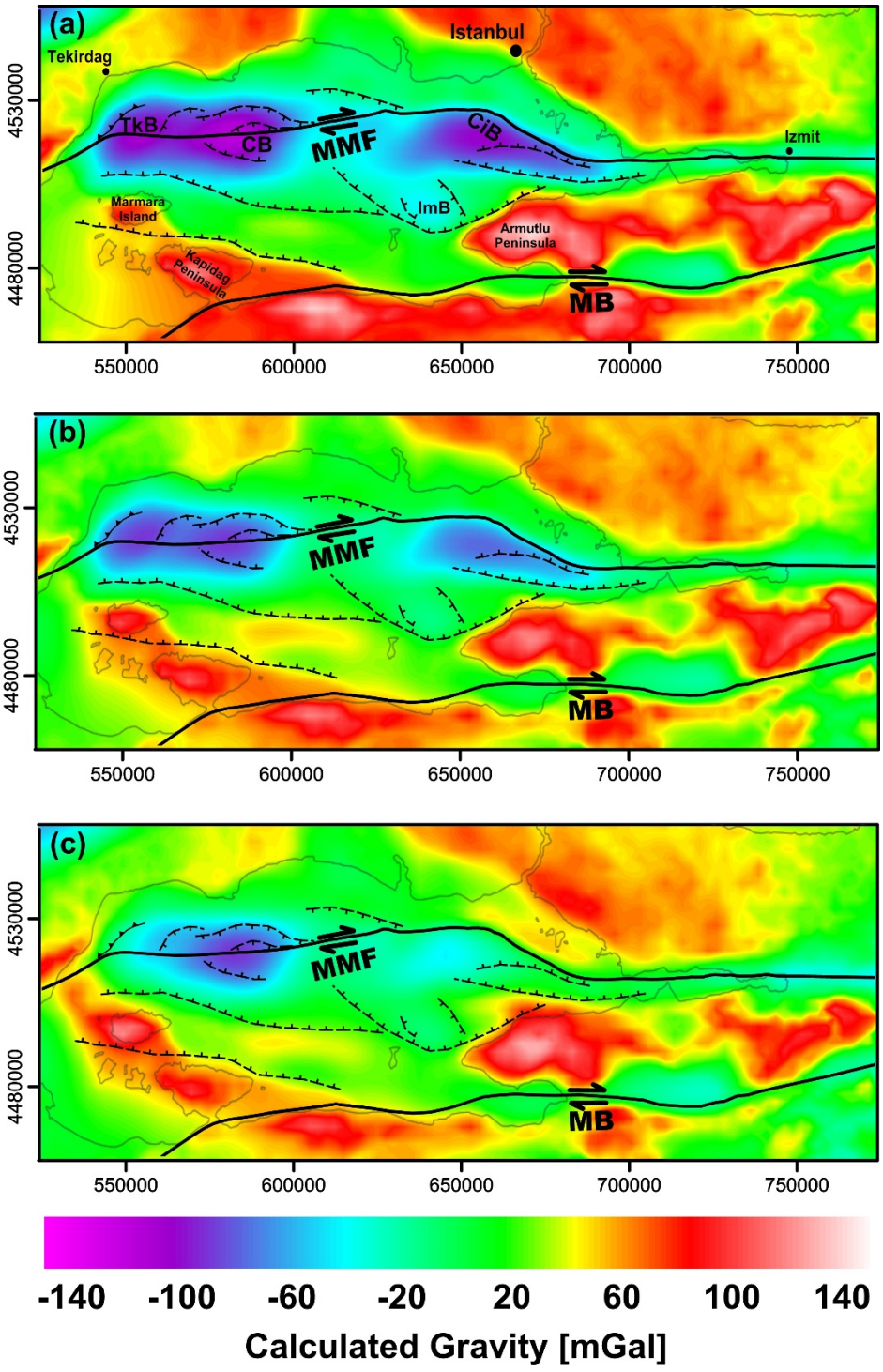
(a)
Istanbul
Tekirdag
TkB
CB
MMF
CiB
Izmit
Marmara Island
ImB
Armutlu Peninsula
Kapidag Peninsula
MB
(b)
MMF
MB
(c)
MMF
MB
4530000
4480000
550000
600000
650000
700000
750000
-140
-100
-60
-20
20
60
100
140
Calculated Gravity [mGal]

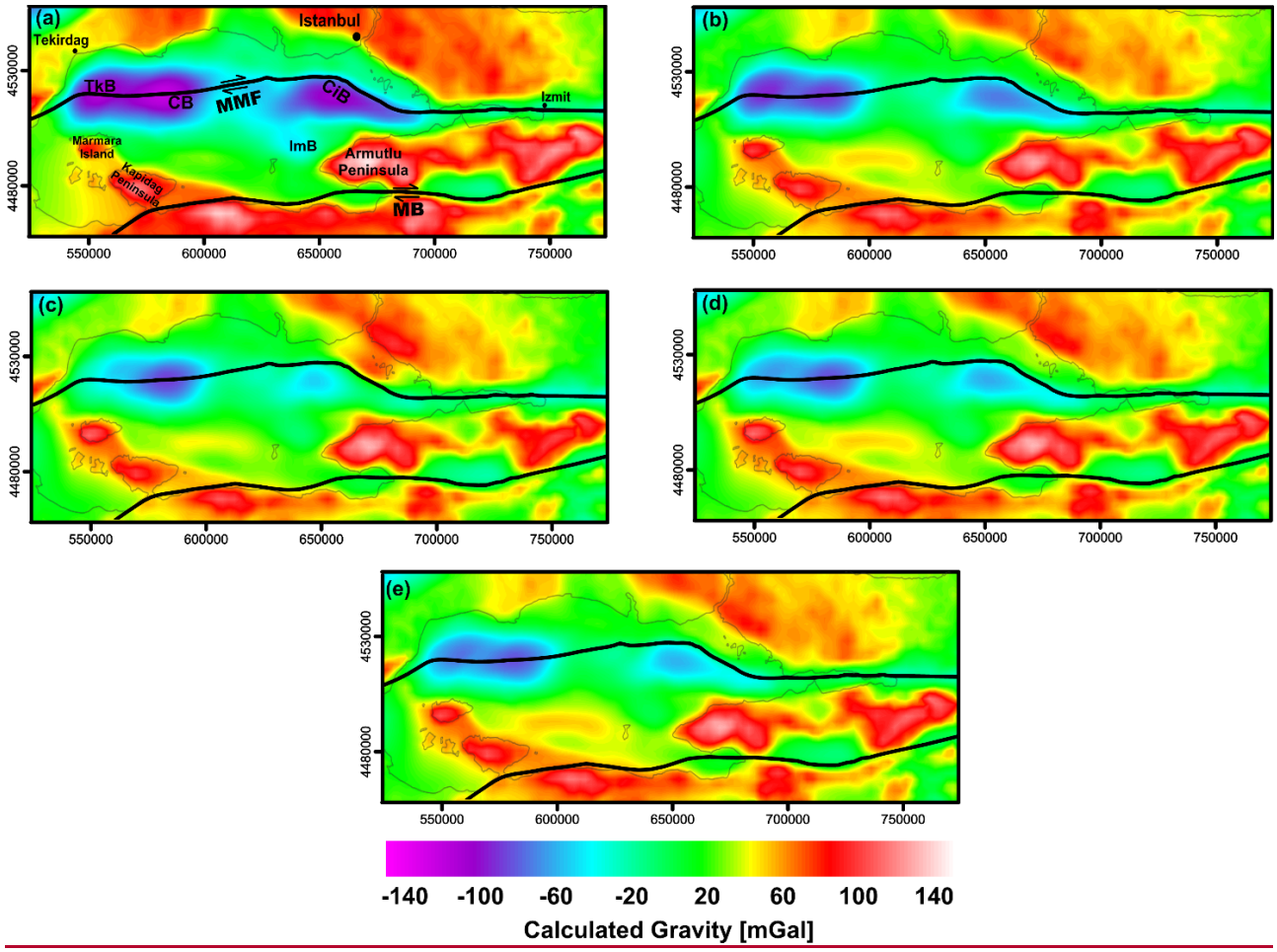


**Figure ~~6~~7: Calculated gravity over the model area (WGS84 UTM Zone 35N): (a) Initial model gravity response; (b) Gravity response of a model with differentiated crust based on the seismic observations (Fig. ~~5~~4); (c) Gravity response of Model-I, the best-fit model based on the forward gravity modelling~~.~~ on Eigen-6C4 (Förste et al., 2014); (d) Gravity response of Model-II, the best-fit model based on the forward gravity modelling on Improved–TOPEX (Kende et al., 2017); (e) Gravity response of Model-III, the alternative best-fit model based on the forward gravity modelling on Improved–TOPEX (Kende et al., 2017). The average density for the modelled high-density bodies is 3150 kg.m$^{-3}$ in Model-I and Model-II, and 2890 kg.m$^{-3}$ in Model-III. The corresponding residual gravity anomaly of each model is shown in Fig. ~~7~~8.**

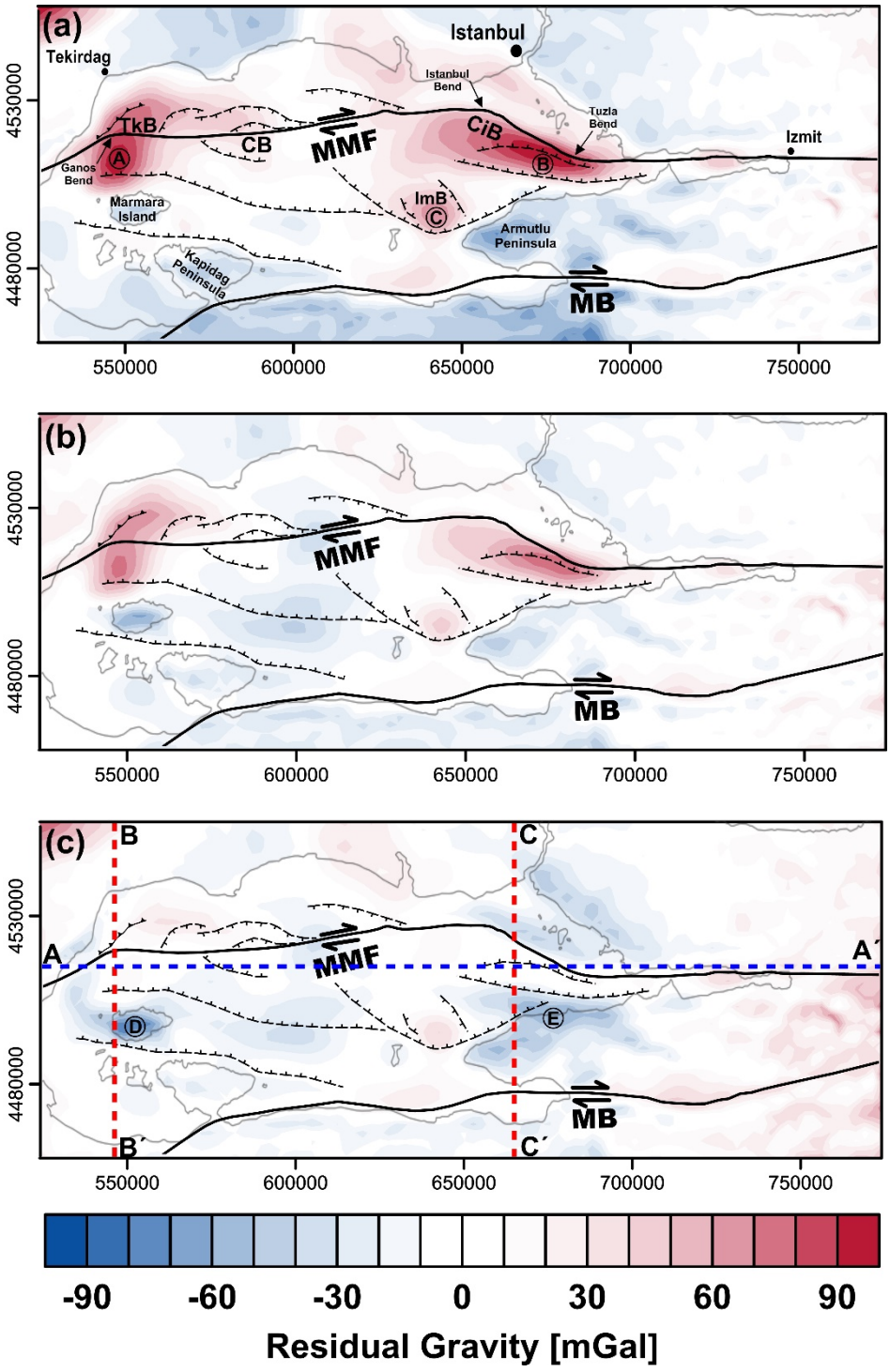
(a)
Istanbul
Tekirdag
Istanbul Bend
Tuzla Bend
Izmit
TkB
CB
MMF
CiB
Ganos Bend
A
B
ImB
C
Marmara Island
Armutlu Peninsula
Kapidag Peninsula
MB
4530000
4480000
550000
600000
650000
700000
750000
(b)
MMF
MB
(c)
B
C
A
A´
D
E
B´
C´
-90
-60
-30
0
30
60
90
Residual Gravity [mGal]

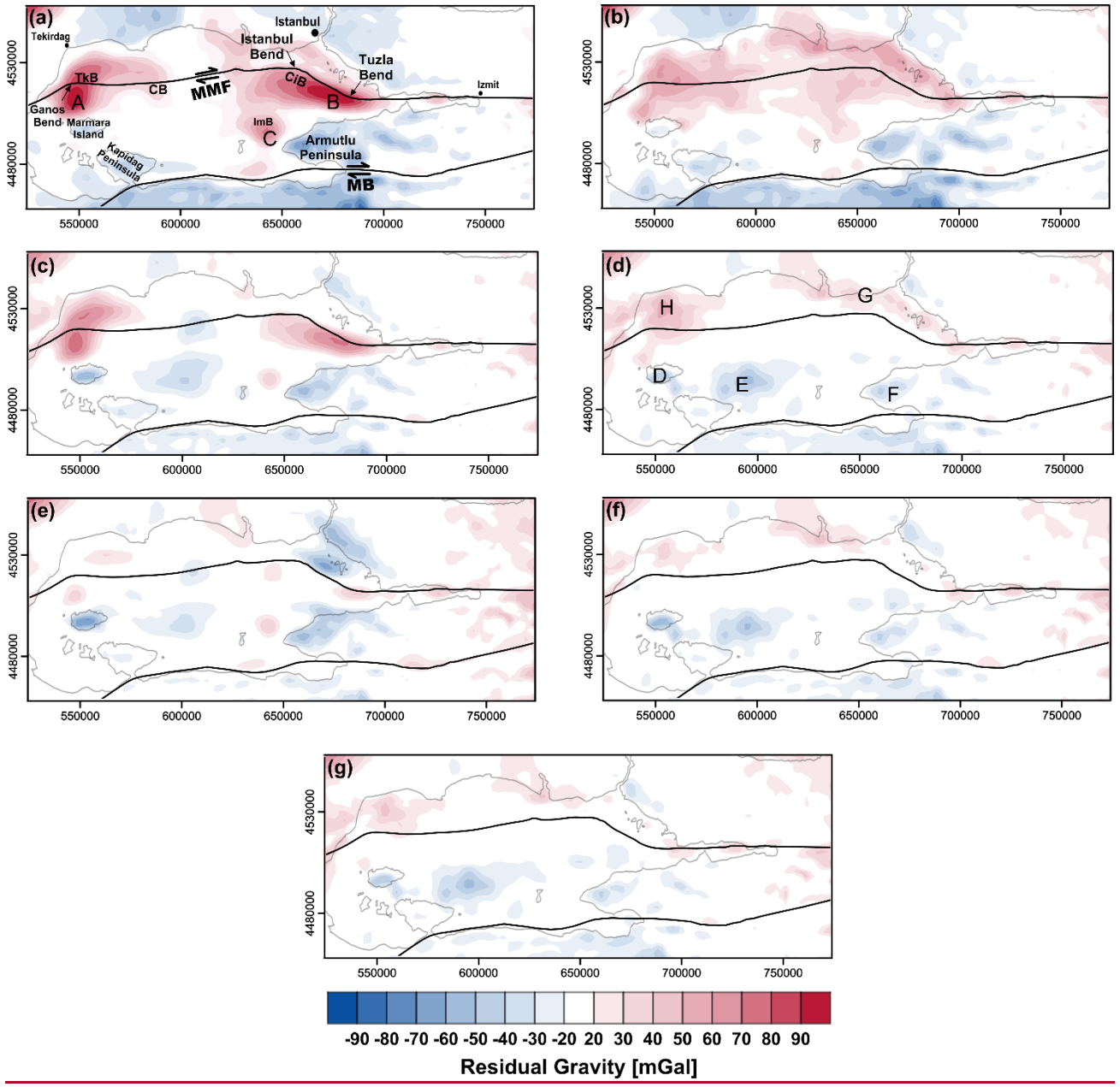


**Figure ~~7~~8: Residual gravity anomaly maps show the misfit between the observed (Fig. ~~4~~a5) and calculated gravity (Fig. ~~6~~7) of different structural model across the study area (WGS84 UTM Zone 35N): (a) Initial model~~;~~ to Eigen-6C4 (Förste et al., 2014); (b) Initial model to Improved–TOPEX (Kende et al., 2017); (c) Model with a differentiated crustal unit~~; (c) Best-fit model~~ to Eigen-6C4; (d) Model with a differentiated crustal unit to Improved–TOPEX; (e) Model-I, the best-fit model based on the ~~3D~~ forward gravity modelling~~. AA´, BB´,~~ on Eigen-6C4; (f) Model-II, the best-fit model based on the forward gravity modelling on Improved–TOPEX; (g) Model-III, the alternative best-fit model based on the forward gravity modelling on Improved–TOPEX. The average density for the modelled high-density bodies is 3150 kg.m$^{-3}$ in Model-I and ~~CC´ show the location~~ Model-II, and 2890 kg.m$^{-3}$ in Model-III.**

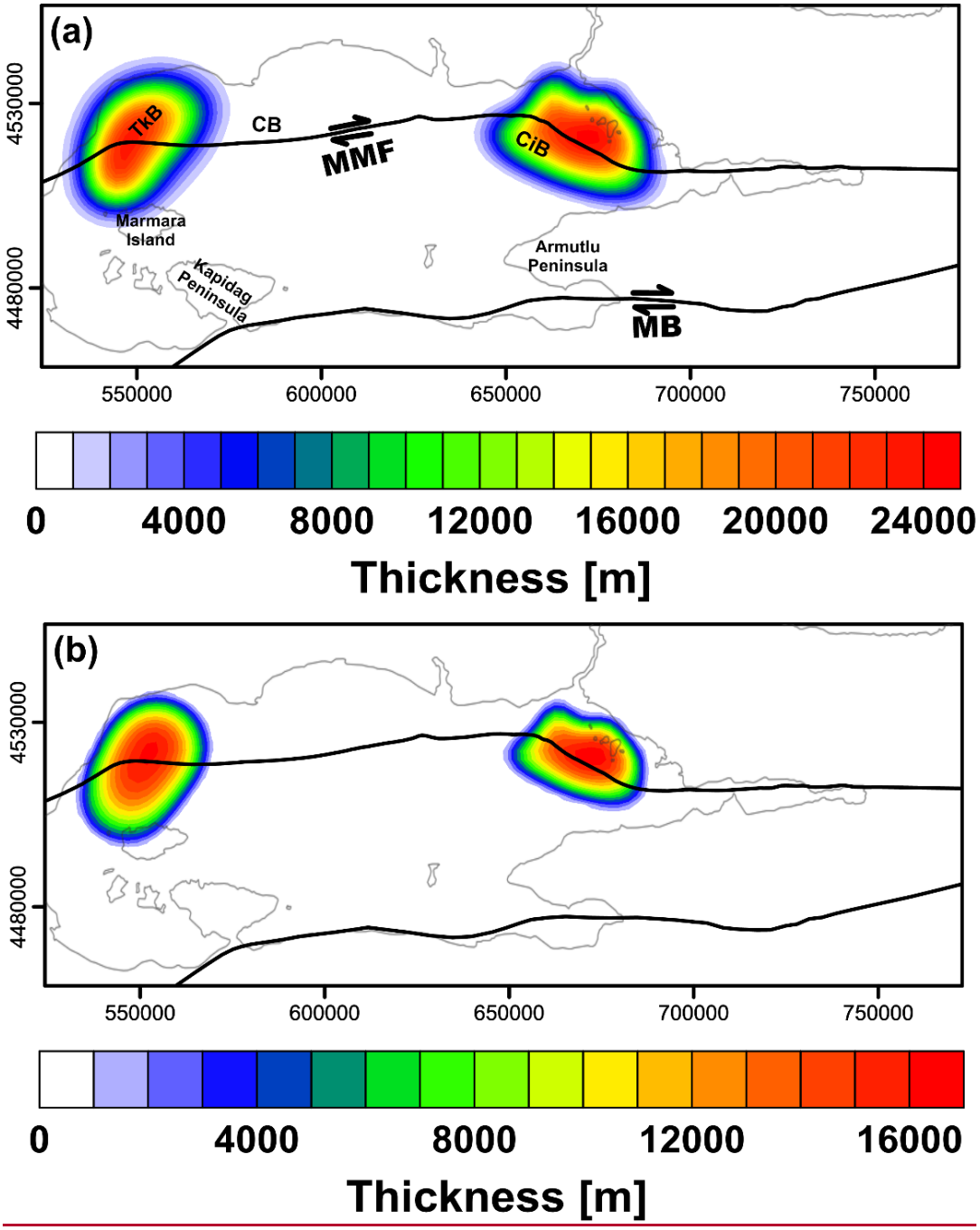


**Figure 9: Thickness of the ~~cross-sections in Fig. 8.~~high-density bodies achieved from the forward gravity modelling: (a) This thickness map represents the high-density bodies that presents the best-fit with an average density of 3150 kg.m$^{-3}$ to EIGEN-6C4 (Model-I) and of 2890 to Improved-TOPEX (Model-III); (b) Thickness of high-density bodies with an average density of 3150 kg.m$^{-3}$ that shows the best-fit to Improved-TOPEX (Model-II).**

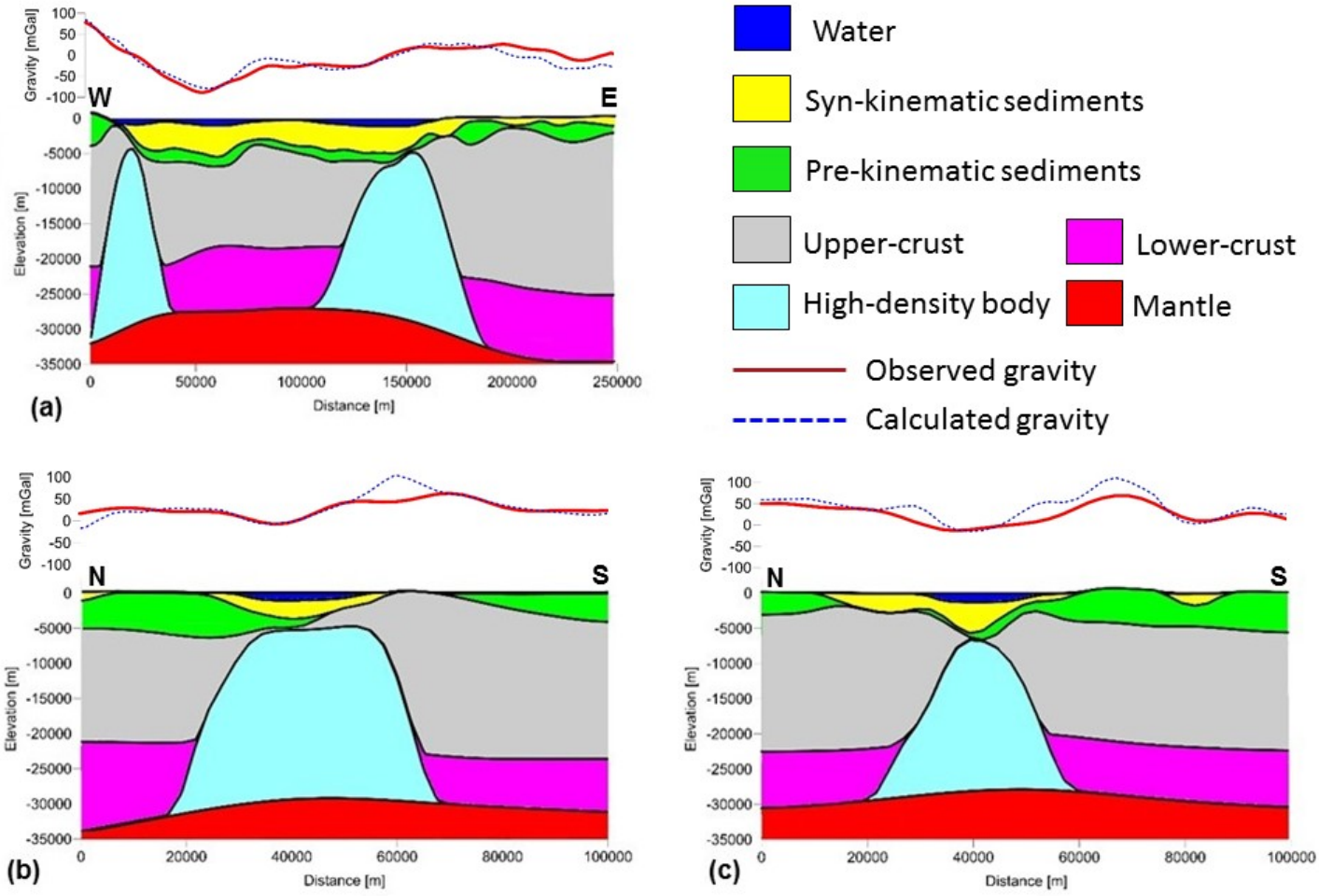
Gravity [mGal]
100
50
0
-50
-100
W
E
Elevation [m]
0
-5000
-10000
-15000
-20000
-25000
-30000
-35000
0
50000
100000
150000
200000
250000
Distance [m]
(a)
Water
Syn-kinematic sediments
Pre-kinematic sediments
Upper-crust
Lower-crust
High-density body
Mantle
Observed gravity
Calculated gravity
N
S
0
20000
40000
60000
80000
100000
(b)
(c)

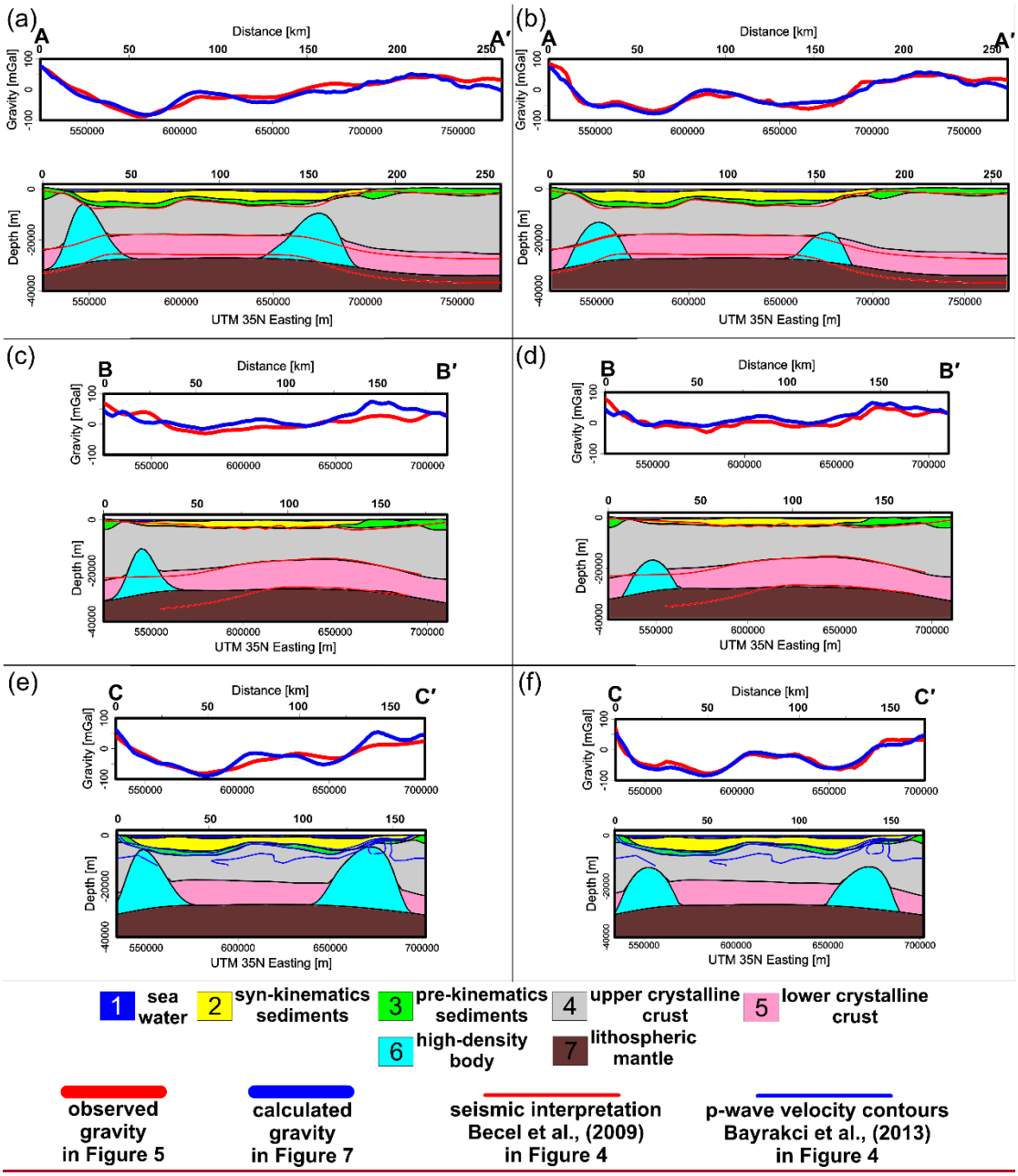


Figure ~~8~~10: Cross-sections ~~of~~for alternative best-fit density models to the two different gravity datasets including high-density bodies with an average density of 3150 kg.m$^{-3}$ (Model-I and Model-II) with the observed and calculated gravity

~~based on~~and the seismic information along the AA′, BB′, CC′ profiles in Fig. 4. Model-I shows the best-fit gravity model ~~and the corresponding structural settings. The profile locations are shown in Fig. 7c: (a) AA´; (b) BB´; (c) CC´.~~

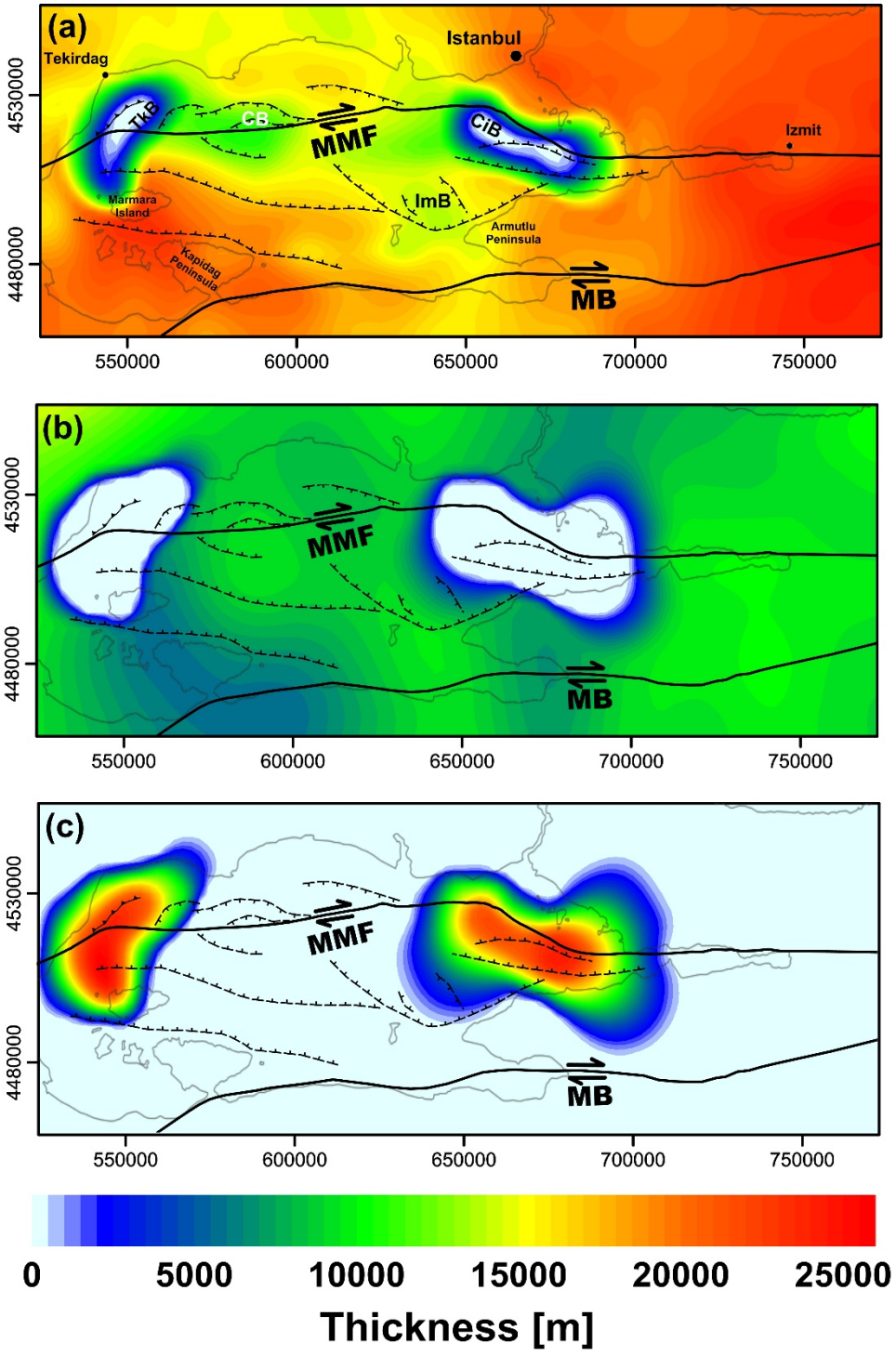

**~~Figure 9: Thickness map of different units of the crystalline crust based on~~to EIGEN-6C4 dataset (Förste et al., 2014) and Model-II represents the best-fit gravity model ~~(WGS84 UTM Zone 35N~~to Improved–TOPEX dataset (Kende at al., 2017): (a) ~~Upper crystalline crust~~Model-I; (b) ~~Lower crystalline crust~~Model-II; (c) ~~High-density bodies.~~**

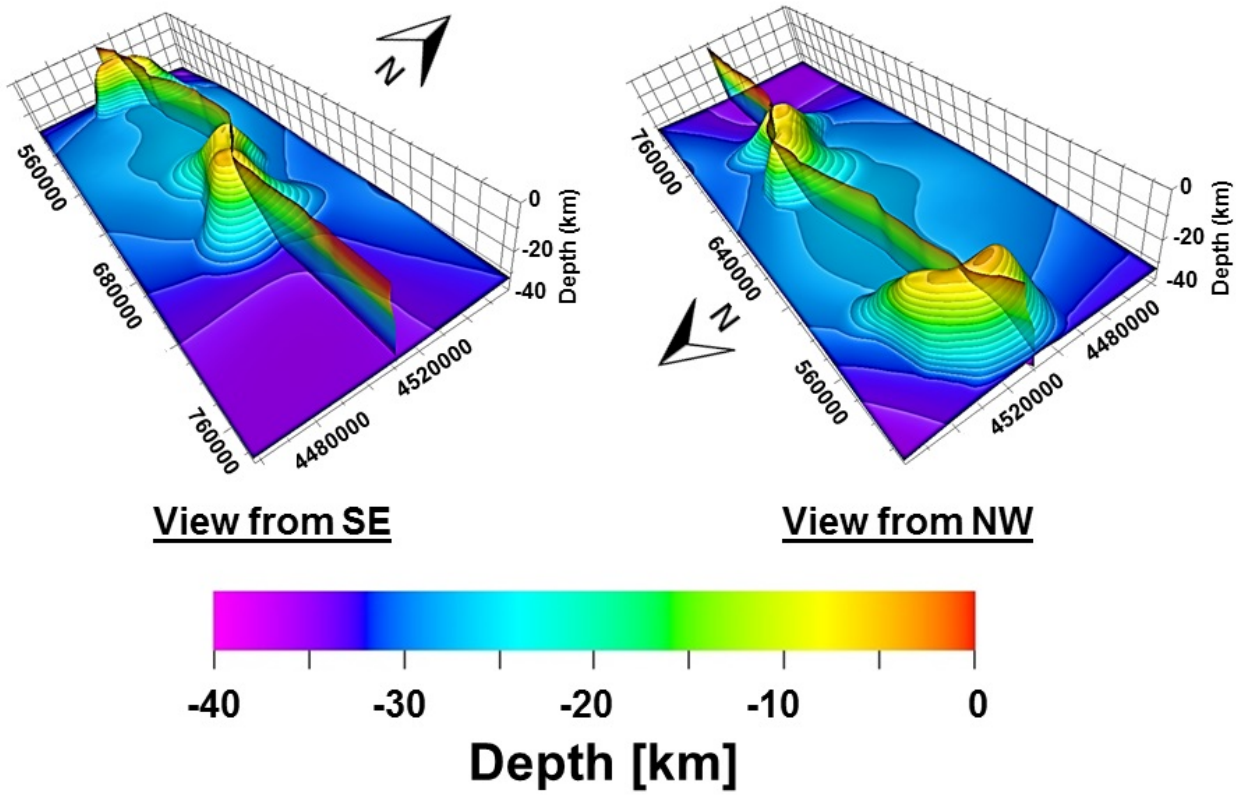


**Model-I; (d) Model-II; (e) Model-I; (f) Model-II.**

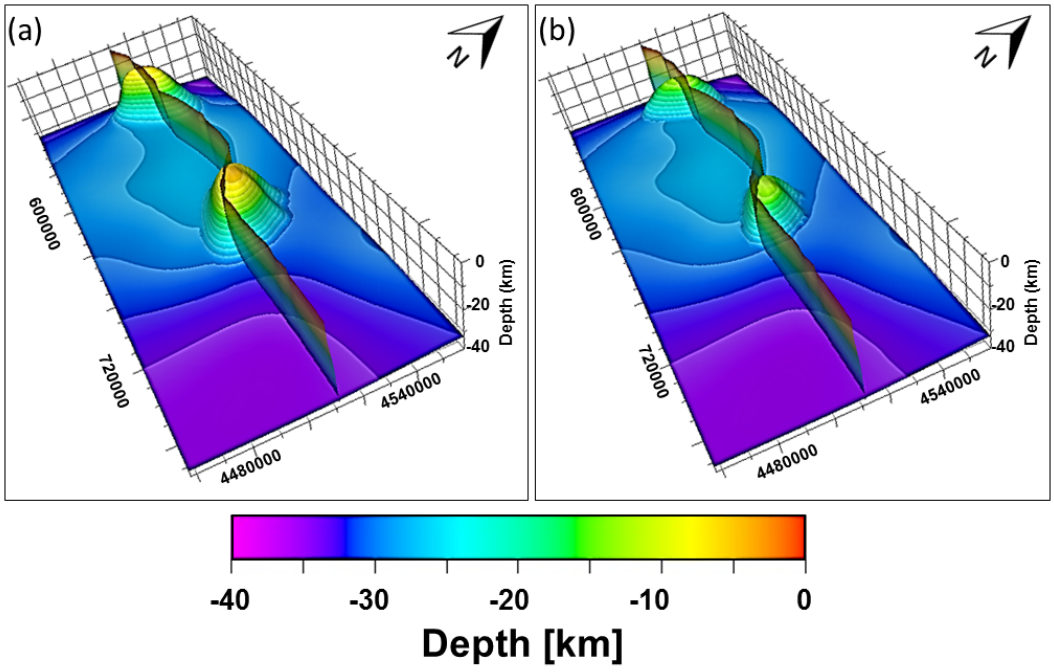


**Figure ~~10~~11: 3D view of the Moho, the high-density bodies, and the MMF plane across the model area (WGS84 UTM Zone 35N). The high-density bodies location spatially correlates with the bent segments of the MMF~~.~~: (a) High-density bodies according to Model-I and Model-III with an average density of 3150 and 2890 kg.m$^{-3}$, respectively; (b) High-density bodies according to Model-II with an average density of 3150 kg.m$^{-3}$. The Moho depth and the 3D fault plane from Hergert and Heidbach (2010).**

**Table 1: Structural units resolved in three alternative density models (Model-I, Model-II, and Model-III) of the Sea of Marmara with interpreted lithology and corresponding physical properties ~~and interpreted lithology~~. The seismic velocity and density relationship is based on the Eq. 1 (Brocher, 2005). Note that the high-density bodies have not yet been ~~(yet)~~ imaged by seismic observations, and their physical properties are according to the density modelling.**

| Structural Units | Average P-wave Velocity ($m.s^{-1}$) | Average Density ($kg.m^{-3}$) | Lithological Interpretation |
|---|---|---|---|
| Seawater | – | 1025 | – |
| Syn-kinematic Sediments | 2250 (1800 to 4200)† | 2000 (1700 to 2300)* | Clastic sediments (poorly consolidated) |
| Pre-kinematic Sediments | 4700 (4200 to 5200)† | 2490 | Sediments (consolidated) |
| Upper crystalline crust | 6000 (5700 to 6300)‡ | 2720 | Felsic metamorphic (biotite gneiss, phyllite)• |
| Lower crystalline crust | 6700‡ | 2890 | Intermediate to Mafic (diorite, granulite)• |
| High-density bodies | ~~7275~~7550 / 6700 (?) | ~~3050~~3150 (Model-I & Model-II) / 2890 (Model-III) | Mafic / Intermediate to Mafic (gabbroic intrusive / diorite, granulite)• |
| Mantle | 8000‡ | 3300 | – |

*†: Bayrakci et al., 2013; *: Hergert et al., 2011; ‡: Bécel et al., 2009; ●: Christensen and Mooney, 1995*